Loss of HP1α alters nuclear integrity to promote cellular invasion

A thesis presented in partial fulfilment of the requirements for the degree of

Master of Science

in

Biochemistry

At Massey University, Manawatū,

New Zealand

Raoul Solomon

2019

Abstract

The onset of invasion is a key step towards the development of metastatic cancer. For a cell to invade through interstitial spaces in the tissue requires a reduction in nuclear rigidity as the cell needs to deform to squeeze through small spaces. Heterochromatin Protein 1α (HP1α) is a protein that defines domains of heterochromatin, the highly compact regions of the genome, and is essential for maintaining the appropriate patterns of gene expression and genome stability. Loss or reduction of HP1α has been correlated with an increase in invasive potential in human tumours.

Using an established model of *Drosophila melanogaster* epithelial cell invasion, the causative role HP1α plays in suppressing cellular invasive is confirmed within an epithelial tissue microenvironment. This model also demonstrates that loss of the *Drosophila melanogaster* HP1 homologue synergistically promotes cellular invasion in conjunction with an activated malignant signalling pathway. Importantly, human HP1α is shown to rescue this highly invasive *Drosophila* phenotype and demonstrates the relevance of this model to human disease, and its use for exploring protein interactions in a cellular microenvironment.

As loss of nuclear integrity has been linked to a reduction in peripheral heterochromatin, the biophysical mechanisms by which HP1α acts as a suppressor of invasive potential were explored in the poorly invasive MCF7 breast cancer cell line with constitutive HP1α knock-down. These cells with reduced HP1α expression had a significant loss of nuclear membrane integrity and stiffness. The underlying nuclear lamina meshwork and associated peripheral heterochromatin was disrupted. This was associated with an increased solubility of lamina proteins, particularly lamin A, as well as the altered localisation of a number of peripheral nuclear proteins. In summary, this work established the important contribution of HP1α to the mechanical integrity of the nucleoskeleton and the role HP1α plays in suppressing malignant signalling pathways that promote cell invasion.

Acknowledgements

Firstly, I would like to enormously thank my Massey University supervisors for their help and guidance without whom this work would not have been completed. Dr Tracy Hale for all her expertise, support, guidance and patience through this work, it has been a true pleasure. Dr Helen Fitzsimons, for her always open door, guidance and tireless creation of fruit flies. Dr Matthew Savoian for his microscopy expertise and support by the Manawatu Microscopy and Imaging Centre.

I would like to thank my collaborators in the biophysical studies, Professor Bill Williams and Susav Pradhan of the Massey School of Fundamental Sciences, and Dr Gleb Yakubov of the University of Queensland, without whom such investigations would have been impossible.

To my colleagues and friends in the Chromatin Research Group and *Drosophila* Neurogenetics laboratory; Lauren McInnes, Ruby Roach, Shannon Ormond, Ana Claasen, Patrick Main and Wei Jun, it has been a delight, you are on fleek.

Finally, to my family, for whom my admiration and gratitude is boundless, thank you.

Table of Contents

List of Figures

List of Tables

Chapter 1: Introduction

1.1: Development of invasive cancer

Fundamentally, cancer is the dysregulation of normal cell growth and survival mechanisms, which leads to uncontrolled cell division accumulation of mutations that would normally trigger programmed cell death. As cell growth continues hyperplastic cells can begin to express increasingly aggressive characteristics, beyond an increased rate of cell division. These hallmarks of these now malignant cells include self-sufficiency in producing growth signals, resistance to growth inhibition signalling, lack of apoptotic response, and the ability to invade both local tissue and metastasise to distal sites. The progression of a benign non-invasive lesion to metastatic malignant tumour is associated with a sharp rise in the rate of morbidity and mortality, as the cancer becomes increasingly drug-resistant and physically harmful to the patient (Kitamura, Qian, & Pollard, 2015). As a result, metastatic cancer remains one of the most challenging medical problems we face today.

For a cell to metastasise it must first undergo major physiological changes to enable it to gain invasive characteristics and migrate through the local tissue microenvironment to reach circulatory systems from which it can spread (Figure 1). Epithelial to mesenchymal transition is a normal cellular process by which differentiated cells lose functional polarity, and revert to a mesenchymal-like state, a migratory form that is key in many developmental processes, including generation of numerous tissues within the embryo. This biological mechanism can be exploited by oncogenic pathways in the onset of cancer, causing the loss of cell-cell adhesion to neighbouring cells, restructuring of the cytoskeleton, and large changes in nuclear morphology and heterochromatin organisation (Li & Li, 2015).

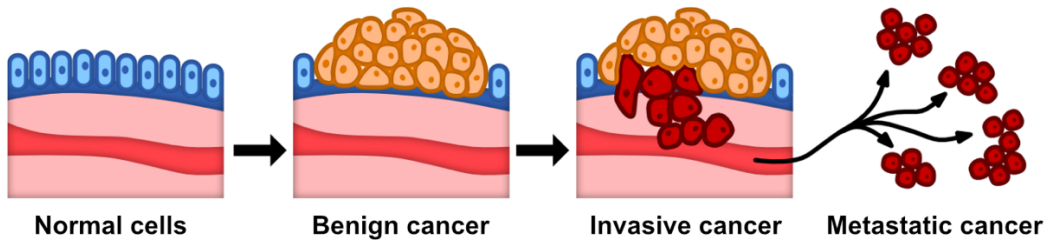

Figure 1: Schematic diagram of stages in development of malignant cells

One of the key determinants of cancer cell migration is an increased ability of a malignant cell to deform and infiltrate through the surrounding tissue. Before migration can occur not only does the cytoskeleton undergo dynamic reorganization, but the nucleus, the largest and stiffest organelle, must become malleable to ensure a cell can squeeze through interstitial spaces (Denais et al., 2016). Thus, complex changes in nuclear shape, position and rigidity are a prerequisite for metastasis and is exemplified by the high-level of nuclear envelope pleomorphism associated with lymph node metastases in breast cancer (Bussolati, Marchiò, Gaetano, Lupo, & Sapino, 2008; Harada et al., 2014).

1.2: The nucleus

The nucleus is the largest organelle in the cell, consisting of a double-membrane lipid bilayer envelope, that encapsulates the genomic DNA that is organised into the nucleoprotein complex known as chromatin. Beneath the inner nuclear membrane lies a dense meshwork of lamina proteins that aid in the formation and support of the membrane.

The nucleus is a major component of cancer identification, as nuclear volume, shape and composition is a key indicator of many cancers, and visual inspection of nuclei is still a key diagnostic tool. Loss of nuclear membrane integrity is associated with increased invasive behaviour (Denais et al., 2016), and increased levels of nuclear pleomorphism and increased elastic properties of the nucleus are required to facilitate invasion in a three-dimensional microenvironment (Bussolati et al., 2008).

1.3: The nuclear envelope

The nuclear envelope partitions the nuclear material from the cytosolic compartment of a cell and is perforated by nuclear pore complexes and other channels to allow exchange between the cytoplasm and the nucleoplasm. The outer nuclear membrane is contiguous with the ribosome rich endoplasmic reticulum and joined intermittently with the inner membrane at nuclear pore complexes (Figure 2). The nuclear pore complexes comprise a major group of proteins that interact with the membrane and occur at junctions between inner and outer nuclear membranes. They allow passive transport of small 30-60kDa proteins, as well the active transport of larger proteins assisted by nuclear transport receptor proteins. The inner membrane interacts with the underlying nuclear lamina network, which is a scaffold structure that plays a major role in nuclear conformation and regulates the association with the nucleoskeleton (Zhang et al., 2001).

There are also a large number of transmembrane proteins embedded in both the inner and outer membranes. These carry out a myriad of signalling roles linking the cytoskeleton to the nucleoskeleton (Vlcek, Dechat, & Foisner, 2001). For example, these include the nesprin protein family that integrate with both inner and outer nuclear membranes and bind to the nucleoskeleton, thus providing a mechanical link between the cytoplasm and the nucleus (Zhang et al., 2001).

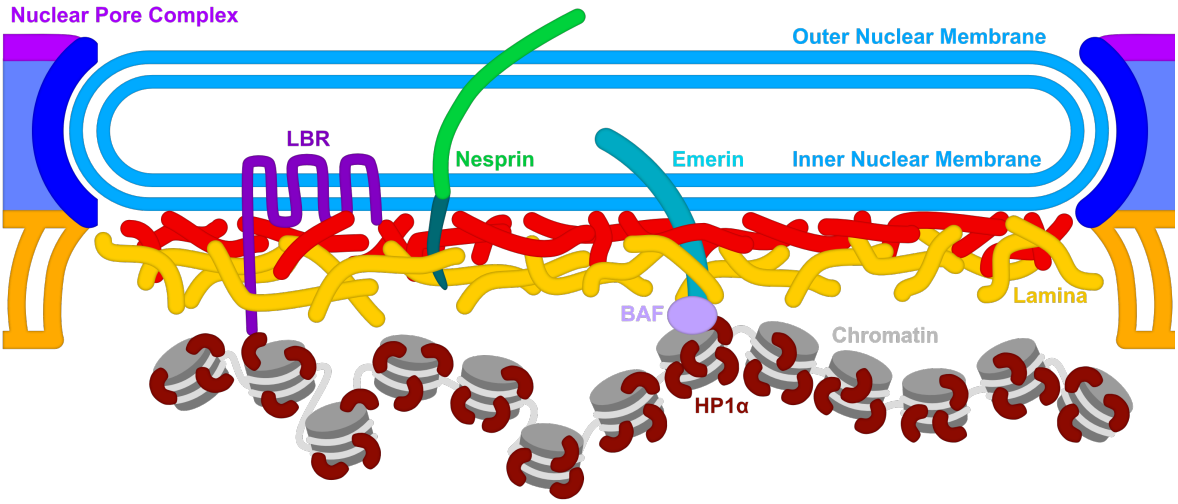

Figure 2: Schematic diagram of the nuclear envelope and nucleoskeleton
The inner and outer nuclear membranes join intermittently at nuclear pore complexes, while beneath the inner nuclear membrane the lamina filamentous network. Peripheral heterochromatin interacts with the lamina and the nuclear membrane through intermediary nuclear membrane proteins, with lamin B Receptor, nesprin and emerin, shown as examples.

1.4: Nuclear lamina

The lamin family of proteins are classed as V intermediate filaments. In humans, there are two A-type lamins, Lamin A and Lamin C which are derived via alternative splicing from the *LMNA* gene, as well as two B-type lamins, B1 and B2 that are transcribed from *LMNA1* and *LMNA2* respectively. Lamins (A, C, B1 and B2) have much stronger expression in highly differentiated cells compared to those that have earlier pluripotent characteristics, indeed lamin A and C tend not to be expressed in human cells until after birth, although the expression ratio between the two types ratio is very dependent on the tissue type, as well as the developmental stage of the cell. The expression of Lamin A and C are frequently altered in tumours, and have been shown to shown to effect malleability (Hutchison, Alvarez-Reyes, & Vaughan, 2001).

Lamins have an intermediate filament structure, characterised by a highly alpha-helical central rod domain flanked by a globular amino-terminal domain, and a long carboxy terminal tail. The tail domain contains a highly conserved s-type immunoglobin (Ig) fold, and a nuclear localisation signal motif between the Ig-fold and the rod domain. Lamins self-assemble into filaments beginning with a parallel coiled-coil dimer, then the dimers assemble into an antiparallel array to form apolar tetrameric filaments, which then associate to 10 nm filaments (Dechat, Adam, Taimen, Shimi, & Goldman, 2010). These filaments display remarkable resistance to fracture as the dimers are able to slide along one another when the filament undergoes intense stretching, up to 60 dyne/cm2 and 90% strain, compared to actin (~35 dyne/cm2 and 20% strain or tubulin (7 dyne/cm2 and 70% strain) (Janmey, Euteneuer, Traub, & Schliwa, 1991). This flexibility and tensile strength enable the nuclear membrane to endure the pressures it undergoes, from both interior changes as the nucleus expands during cell division as well as exterior tugging from cytoskeletal attachments as the cell migrates

Lamins undergo significant post translational modifications in order to dynamically target and bind membranes and form filamentous networks or remain unpolymerized nucleoplasm proteins. In particular the cysteine residue of the carboxy-terminal –CAAX box of Lamin A, B1 and B2 is farnesylated. The attachment of these small chain hydrophobic isoprenyl groups enable lamin binding to the inner membrane. Lamin B1 and B2 remain permanently farnesylated, however Lamin A undergoes further secondary modification that remove the terminal 15 amino acid residues and the entirety of the carboxy-methyl modifications. Lamin C is 74 amino acids shorter than Lamin A, lacking the -CAAX box entirely, and is never farnesylated. This divergence of A-type lamins and the B type may indicate that B lamins would have a stronger and less variable interaction with the membrane due to the additional lipid anchors. The meshwork of lamina formed by the two types appear as distinct filamentous networks, each with their own separate- though interacting- regions (Shimi et al., 2008). In a typical cell, there is a very low degree of mobility of subunits within the filaments, however the mobility and organisation of the lamin network itself, particularly lamin A is influenced by the expression of lamin B1. Silencing of lamin B1results in the increased mobility of the nucleoplasmic lamin A as well as formation of lamin A/C blebs along the membrane that are strongly associated with gene rich chromatin domains that undergo promoter proximal stalling and are transcriptionally inert.

The nuclear envelope needs to be dismantled as the cell enters mitosis. This depolymerisation of the lamina is driven by Cyclin Dependent Kinase mediated phosphorylation. During telophase lamins are dephosphorylated to enable reassembly of the meshwork (Kuga, Nozaki, Matsushita, Nomura, & Tomonaga, 2010).

1.5: Chromatin organisation

Within the nucleus DNA undergoes several levels of compaction, with association of histones to form the chromatin fibre. At the primary level, DNA wraps around an octamer of core histones (H2A, H2B, H3 and H4) to form a nucleosome. With the binding of the linker histone H1 to the nucleosomal array, it is compacted to 30nm chromatin fibre. Beyond this, architectural proteins organise proteins into domains of transcriptionally active euchromatin and highly compacted transcriptionally silent heterochromatin. The retention of heterochromatin at the nuclear periphery renders the nucleus less malleable in differentiated cells, whereas a more diffuse pattern of stem cell-like heterochromatin increases nuclear plasticity (Dahl, Engler, Pajerowski, & Discher, 2005).

1.6: Heterochromatin

Domains of heterochromatin are defined by trimethylation of histone H3 on lysine 9 and Heterochromatin Protein 1α (HP1α) and enriched with linker protein histone H1 and noncoding RNA. They are regions of little transcriptional activity and are broadly classed as either constitutive of facultative heterochromatin. Constitutive heterochromatin remains transcriptionally inactive throughout the cell cycle and is primarily composed of repeating sequences and is involved in maintaining chromatin structures such as the telomeres and centromeres. Facultative heterochromatin is more dynamic in shifting between transcriptionally active euchromatin to heterochromatin throughout the cell cycle, as transcriptionally active elements are silenced through development and cell differentiation (Haaf & Schmid, 2000).

1.7: Heterochromatin Protein 1

HP1 is a highly conserved protein family, with orthologues also present in *Drosophila*, *Xenopus*, chicken, *Arabidopsis,* yeast, and mammals. In mammals, the HP1 family has three members HP1α, HP1ß and HP1γ. HP1α and HP1ß are constitutively expressed throughout the body and are found associated with heterochromatin as previously described.

The formation and architecture of heterochromatin is largely directed and maintained by the Heterochromatin Protein 1 (HP1) family, also known as the Chromobox Homologue (CBX). HP1 was first observed as a non-histone protein associated with heterochromatin regions in *Drosophila melanogaster* (James & Elgin, 1986). Its role in modulating heterochromatin was established when exploring position-effect variegation (PEV), an effect of chimeric gene silencing in some cells as a result of rearrangement juxtaposing a gene within heterochromatin. This resulted in phenotypes that had a variegated expression of a gene, such as the eye colour determining *white* gene, that when inactivated in some cells by proximity to heterochromatin, resulting in a mixed red and white eye colour in fruit flies. Point mutation of the chromodomain of HP1 in these flies removed the PEV phenotype, as heterochromatin formation was inhibited and the silencing of juxtaposed genes did not occur (Eissenberg et al., 1990).

HP1 has a general tripartite structure containing an N-terminal chromodomain, a C-terminal chromoshadow domain, linked by an unstructured hinge region as shown in Figure 3. The chromodomain contains motifs that promote binding in response to nucleosome H3K9 trimethylation, while the chromoshadow domain allows dimerization of HP1 molecules as well as a wide variety of other protein binding partners through the PxVxL motif. The unstructured hinge region binds nucleic acid sequences and histone H1 on chromatin.

HP1α mediates chromatin compaction by binding to trimethylation of lysine 9 of histone H3 and lysine 26 of histone 1.4 (Nishibuchi & Nakayama, 2014). Heterodimerisation and homodimerisation of multiple HP1 binding within the chromoshadow domain draws neighbouring nucleosomes together, compacting the DNA and excluding transcription factors and silencing gene expression (Norwood et al., 2006). Heterochromatic regions spread as HP1α associates with methyltransferases such as SUV39H1 via the chromoshadow domain, which lay down further epigenetic markers, such as trimethylation of histone 3, lysine 9 (H3K9) and lysine 26 of histone 1.4 (H1.4K26) that recruit additional HP1α molecules, resulting in an expanding region of compacted chromatin (Peters et al., 2001) (Nishibuchi & Nakayama, 2014).

The unstructured hinge region of the HP1α molecule, binds both DNA and RNA for the purpose of targeting HP1α to specific regions of the chromosome (Meehan, Kao, & Pennings,

2003). An example of this is Telomere-Repeat-Encoding RNA (TERRA), which is non-coding RNA that is transcribed along the length of the telomere regions of DNA, interacting with HP1α and localising it to the telomeres (Deng, Campbell, & Lieberman, 2010; Deng, Norseen, Wiedmer, Riethman, & Lieberman, 2009).

Recent work has demonstrated how the multivalent interactions of HP1α results in a shift from soluble HP1α to phase separated droplets of protein that nucleate and propagate across chromatin regions. This liquid property of HP1α, and the associated chromatin it is bound to, provides a model for heterochromatin domain formation, wherein free HP1α forms many multivalent interactions with histone components and other HP1α molecules forming foci of concentrated protein that grow larger following further recruitment of HP1α and a phase shift occurs as HP1α becomes insoluble. Heterochromatin domains mature as large foci of HP1α fuse like liquid droplets, bringing distal DNA regions into contact (Larson et al., 2017).

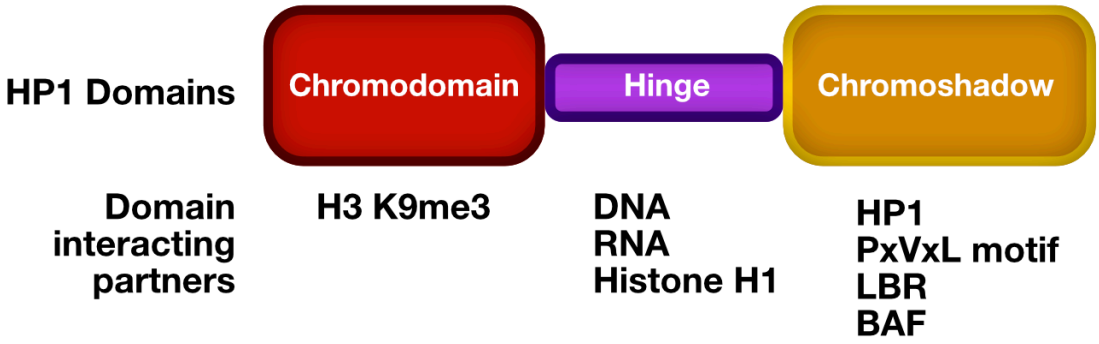

Figure 3: Schematic of HP1 domain structure
Shown is the chromodomain and the chromoshadow domain linked by the hinge region. Below are some binding partners for each domain.

Mechanisms to reverse the condensing effect of HP1α and mediate the decompaction of chromatin to allow transcription are at play throughout development and cell life. Such agonists of HP1α binding include phosphorylation of histone proteins, such as H3S10, which prevents H3K9 methylation, and phosphorylated STAT protein (Rea et al., 2000; Shi et al., 2006).

1.8: HP1 dysregulation in cancer

There is strong evidence that HP1 has a role in tumour suppression. The loss of HP1 function enhances the oncogenic potential of JAK/STAT over-expression in a *Drosophila* model, while its reintroduction reduces the number of lesions (Shi et al., 2006). In humans, a causal role in tumour invasion has been demonstrated by the modulation of HP1α levels (Norwood et al.,

2006). Knock-down (KD) of HP1α mRNA in poorly invasive/non-metastatic cells increased invasion, without changes in cell growth rate (Norwood et al., 2006). Conversely, over-expression of HP1α can suppress the metastatic potential of invasive breast cancer cell lines, suggesting HP1 is a suppressor of metastasis (Norwood et al., 2006). This observation was supported by immunohistochemistry studies showing low levels of HP1α protein in seven of nine invasive breast tumours (Dawn A Kirschmann et al., 2000). In addition, cDNA microarray studies show correlation of decreased HP1α mRNA expression with tumour progression in advanced papillary thyroid carcinomas (Wasenius et al., 2003) and medulloblastomas (Pomeroy et al., 2002). In the latter case this down-regulation correlated with treatment failure.

While generally ubiquitous in normal tissue, differential expression of the HP1 paralogs has been observed in both human tumour derived cells and tissues (Kirschmann, Seftor, Nieva, Mariano, & Hendrix, 1999; Ritou, Bai, & Georgatos, 2007) For example, while expression of the paralogs varies with the tumour context in solid tissue, generally increased expression is observed in tumours with poor outcome. For example, upregulation of HP1γ is associated with poorly differentiated colorectal tumours (M. Liu et al., 2015), upregulation of HP1β is associated with increasing grade in prostate cancers (Shiota et al., 2010), and upregulation of HP1α expression has been observed in non-metastatic breast carcinomas compared to normal tissue (De Koning et al., 2009) and glioma cells (Lai, Deng, Guo, Zhu, & Tu, 2017). This increase in expression has been proposed to maintain genome stability in cells with a high proliferative demand and is therefore advantageous during the early stages of tumour development.

Reduction of the heterochromatin-enriched paralogs has also been observed, with loss of HP1β reported in poorly differentiated colon cancers (Tell et al., 2011), invasive melanoma lesions (Nishimura, Hirokawa, Mizutani, & Shiraishi, 2006), thyroid carcinomas (Tretiakova et al., 2014) and prostate cancer (Shapiro et al., 2008). HP1α levels are dramatically reduced in breast metastatic lesions from distant sites in the body (Dawn A Kirschmann et al., 2000), and its loss is correlated with metastatic potential and poor outcome in advanced papillary thyroid carcinomas (Tretiakova et al., 2014; Wasenius et al., 2003), in addition HP1α is suggested to reduce metastasis in colorectal cancer (Ruginis, Taglia, Matusiak, Lee, & Benya, 2006). This correlation of HP1α down-regulation with an invasive tumour phenotype and the demonstration that HP1α can regulate the invasive potential of breast cancer cell lines has led

to the proposal that HP1α is a suppressor of breast metastasis (Dawn A Kirschmann et al., 2000; Norwood et al., 2006).

Indeed, the onset of invasion correlates with the loss of HP1α in many solid tumours including those of the thyroid, kidney, colon and breast (Contreras, Gutierrez, & Hale, 2010; Dawn A Kirschmann et al., 2000; Tretiakova et al., 2014). Screening of a tissue microarray containing 56 invasive breast carcinomas showed that 32 out of the 56 breast carcinomas had decreased expression of HP1α. That HP1α can suppress invasion is demonstrated by its modulation in malignant breast cells altering cellular adhesion and migration through a 3-D matrix (Hale, Wheeler, Stimpson, Tretiakova, & Contreras, 2016; Norwood et al., 2006). In the poorly invasive breast MCF7 cell line constitutive KD of HP1α was shown to increase the cells' ability to invade through an extracellular matrix by 44%. Conversely, introduction of HP1 α in the highly invasive MDA-MB-231 breast cancer cell line (with low endogenous levels of HP1α) decreased their ability to invade by 40%.

1.9: Object of this work is to establish whether HP1*α* plays causative role in increasing nuclear malleability

The HP1α protein plays a vital role in the formation and maintenance of the heterochromatin, and its loss in both cell lines and *in vivo* is associated with increased invasive potential. In conjunction with the invasive model in *Drosophila,* investigations into the role that is played by the nuclear membrane itself in facilitating invasive characteristics, modulated by HP1α and nuclear envelope associated proteins such as lamin A, C, B2 and B1, as well as other candidate proteins, will provide valuable insight into the biophysical behaviour of invasive cancers. Loss of nuclear membrane integrity is a hallmark of many cancers and is closely linked to the disruption of the nuclear lamina. Loss of peripheral heterochromatin has been shown to destabilise the lamina layer, and so this study will explore if HP1α KD can direct a similar loss of nuclear membrane integrity, suggesting a structural mechanism by which HP1α modulates invasive development, beyond its role in gene regulation. This has the potential to characterise targets for future cancer markers, predictors and therapies.

Chapter 2: Materials and Methods

2.1: Generation and maintenance of *Drosophila melanogaster* lines /Generation of ptc-driven GFP and RNAi KD *Drosophila melanogaster*

Drosophila melanogaster were cultured on a standard medium (agar (1%, w/v), yeast (4% w/v), cornflour (11%, w/v), sugar (13%, w/v), molasses (2%, v/v), methylparaben (0.33%, w/v), ethanol (37 % v/v)) and raised at 22C, unless otherwise indicated, with a 12-hour light-dark cycle. All fly stocks were obtained from the Bloomington *Drosophila* Stock Centre (BDSC), the Vienna *Drosophila* Resource Centre (VDRC), or generated in house, as indicated below. This work has ERMA approval for creation of genetic modified organisms that are necessary for this research - GMO09/MU003 and GMC00017.

In order to visualise the A/P boundary of the imaginal disc, a fly line containing the Ptc-Gal4 driver (BDSC# 2017) and UAS-GFP (BDSC #6874) was created. This fly line was then crossed with lines containing UAS-linked RNAi and/or transgenes to KD or overexpress genes of interest in the A/P epithelial stripe.

The Ptc-GAL4 and UAS-GFP constructs are both inserted on chromosome two. In order to create lines that are homozygous for both Ptc-GAL4 and UAS-GFP, homozygous Ptc-GAL4 males were firstly crossed to homozygous UAS-GFP homozygous females to produce heterozygous progeny carrying one copy of each gene (Figure 4A). Homologous recombination occurs only in female *Drosophila*, therefore female progeny resulting from this cross were selected and crossed to control (*w*-) males (Figure 4B). Both ptc-GAL4 and UAS-GFP are linked to the mini-white gene (*w*+) which is a determinant of eye colour, and the eye colour (ranging from light yellow to red) is dependent on the level of expression of *w*+. Flies heterozygous for ptc-GAL4 or UAS-GFP have orange eyes, therefore most of the progeny from this cross will have orange eyes with a single copy of either Ptc-Gal4 (ptc-GAL4/+) or UAS-GFP (UAS-GFP/+), however in instances where recombination has occurred, flies will exhibit red eyes as both of the constructs have been recombined onto a single chromosome (UAS-GFP,UAS-GAL4/+) (Figure 4B). A comma between the two genetic elements indicates they are on the same chromosome, whereas a forward slash indicates they are on opposite copies of chromosome two. The "+" indicates a wild-type chromosome.

To create a stable homozygous stock, male red-eyed progeny of Figure 2.1B were crossed with *w*- female flies containing the CyO second chromosome balancer. (Figure 4C). Balancer chromosomes contain a number of balanced chromosomal inversions which prevent

recombination, as well as carrying a dominant phenotypic marker to track the chromosome presence, in this case curly wings. The resulting progeny were selected for red eyes and curly wings, indicating the presence of Ptc-GAL4 and UAS-GFP over the balancer chromosome (Ptc-GAL4, UAS-GFP/CyO).

To create the final fly stock that is homozygous for ptc-GAL4 and UAS-GFP (ptc-GAL4, UAS-GFP), red-eyed and curly winged male and female progeny were crossed together, and non-curly progeny were selected (Figure 2.1D). The balancer chromosome is homozygous lethal; therefore, no white-eyed non-curly progeny were produced. The presence of UAS-GFP and Ptc-GAL4 was confirmed by dissecting the imaginal discs and visualising GFP expression in the A/P boundary.

A homozygous fly line harbouring both UAS-HP1 RNAi (VDRC #31994) and UAS-Csk RNAi (VDRC #32877) on chromosome two was generated using the same method as described above. Similarly, a UAS-HP1 overexpression fly line (UAS-HP1OE, as described in Section 3.1.2) was recombined with UAS-HP1 RNAi (VDRC #31994) to create a homozygous line carrying UAS-HP1 RNAi and UAS-HP1 OE. The generation of all the above-mentioned fly lines was performed by Dr Helen Fitzsimons,

To generate the experimental set of larvae of the required genotypes, five virgin Ptc-Gal4,UAS-GFP females were crossed with five males of the appropriate transgenic lines (i.e. such as UAS-Csk RNAi) to produce progeny that contained one copy of each of UAS-GFP and ptc-GAL4 to visualise the A/P stripe, as well as one copy of the desired UAS-RNAi or UAS-OE construct(s), the expression of which was also driven by ptc-GAL4.

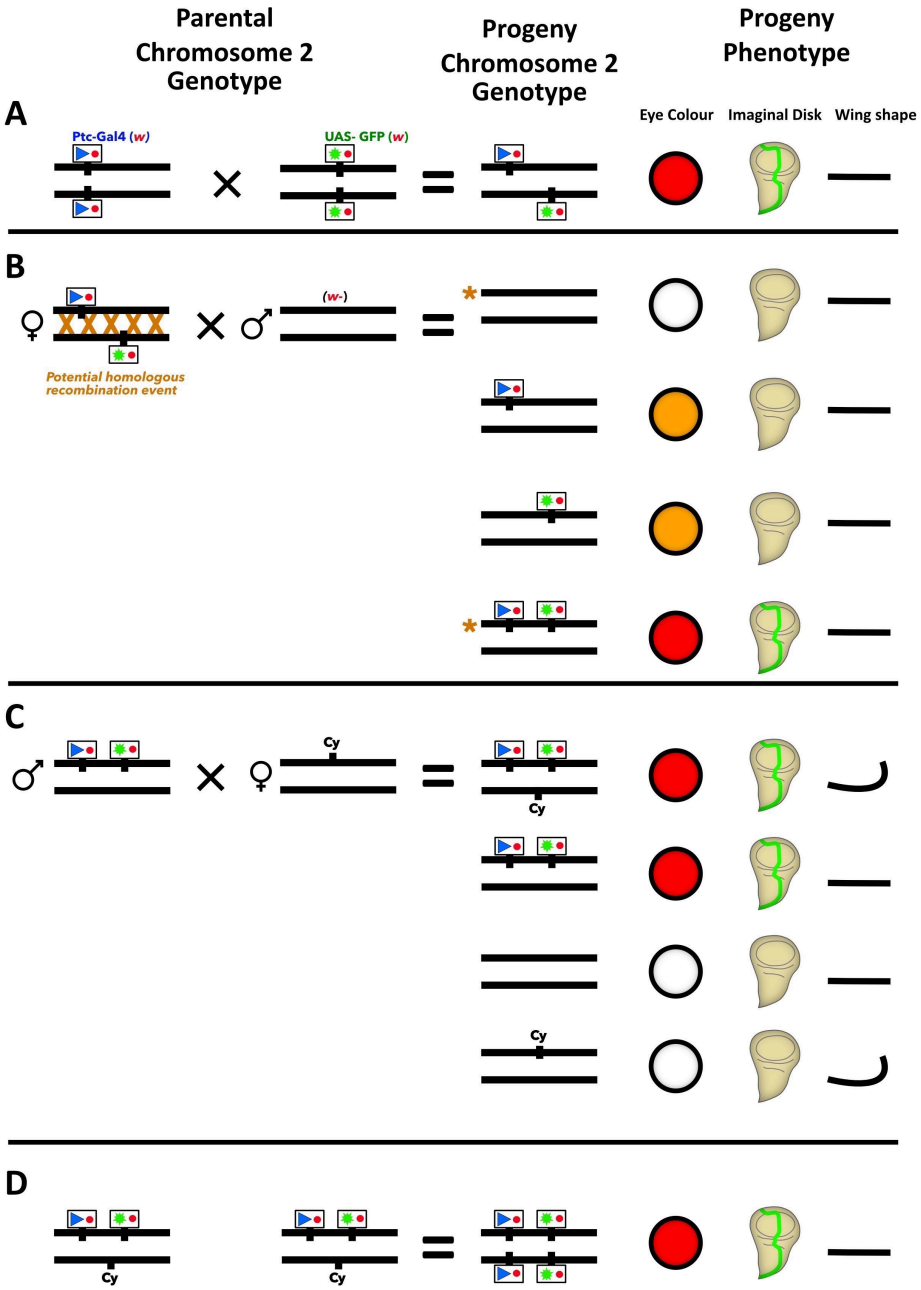

Figure 4: Genotype crossing to produce stable Ptc-Gal4/UAS-GFP *Drosophila* line
Schematic of chromosome two genotypes of parental fly lines, and the genotypes and key phenotypes of their potential progeny. Phenotypes are identified as eye colours ranging from white to yellow to red depending on *white* gene dosage, imaginal disc fluorescence in response to Gal4 activation of UAS-GFP, and either straight or curly wing shape. A) Cross of homozygous Ptc-Gal4 with homozygous UAS-GFP to produce heterozygous offspring. B) Female heterozygous Ptc-Gal4/UAS-GFP crossed with white eyed males (+/+). * indicates a homologous recombination event has occurred, combining both Ptc-Gal4 and UAS-GFP on a single chromosome, leaving no transgenes on one of the chromosome pair. C) Cross of heterozygous recombined progeny from B, with Ptc-Gal4, UAS-GFP on a single chromosome, crossed with a curly balancer to prevent further recombination. D) Cross of heterozygous (Ptc-Gal4, UAS-GFP/CyO) to produce homozygous (Ptc-Gal4, UAS-GFP/ Ptc-Gal4, UAS-GFP).

2.2: Dissection of third instar *Drosophila melanogaster* wing imaginal discs

The isolation of wing imaginal discs was carried out following a dissection protocol established by(Spratford & Kumar, 2014). Imaginal discs were harvested at the third instar stage of *Drosophila melanogaster* development, at the point they are 'wandering' larvae, that have climbed out of the food media and are actively moving along the growth tube walls, prior to the pupation stage. Selected larvae were transferred from the growth tube and submerged in phosphate buffered saline (PBS) (137 mM NaCl, 2.7 mM KCl, 10 mM Na2HPO4, 1.8 mM KH2HPO4) with 0.05% Triton X-100 to self-cleanse for five minutes. Larvae were then transferred to a drop of PBS on a microscope slide, under a dissection microscope. Using fine forceps to pinch the anterior and posterior outer layer of the larvae, gentle pressure is applied to tear the membrane and allow release of the interior organs. Careful manipulation of the tissue allows identification and removal of the two imaginal discs to another pool of PBS on the slide. After removing the remaining larval tissue, the collected discs were then fixed in a drop of 4% paraformaldehyde in PBS for 25 minutes at room temperature. The fixative solution was removed by blotting, and the discs washed twice by immersing in PBS, before mounting in 1.5 µg/ml VectaShield 4',6-diamidino-2-phenylindole (DAPI) (Vector Laboratories Catalogue Number: H-1200), cover-slipped and stored at 4ºC before imaging.

2.3: Immunohistochemistry *Drosophila melanogaster* wing imaginal discs

Wandering third instar larvae of the appropriate genotypes were dissected to collect the wing imaginal discs, which were immediately transferred to a cold fixative solution (2% Paraformaldehyde, 15µM Sodium Periodate, 140µM Lysine in PBS) for 45 minutes at room temperature. The imaginal discs were then incubated in a permeabilization buffer (0.1M Sodium Phosphate, 0.5% Triton TX100) for 45 minutes at room temperature, then blocked in 10% Normal Goat Serum (NGS) for ten minutes before being incubated overnight at 4ºC in a primary antibody diluted in 10% NGS. Following primary staining, the discs were rinsed in wash buffer (0.1M Sodium Phosphate, 0.2% Triton TX100), before the secondary antibody was applied for four hours. The imaginal discs were then further washed and mounted in VectaShield DAPI (Vector Laboratories: #H-1200).

2.4: Table of *Drosophila melanogaster* genotypes

Integrated DNA	Chromosomal Linkage	Genotype	Phenotype

UAS-Red Stinger (nls.dsRED2)	3	*w[1118];P{UAS-RedStinger}6*	Red eyes
UAS-GFP	2	*w[*]; P{w+mC=UAS-2xEGFP}AH2*	Orange eyes
Csk RNAi	2	*y,w[1118];P{attP,y[+],w[3`]},P{w[+mC]=CG42317}*	Orange eyes
Csk RNAi	3	*w[1118];P{w[+mC]=CG42317*	Orange eyes
HP1 RNAi	2	*y,w[1118];P{attP,y[+],w[3`]},P{w[+mC]=CG8409}*	Orange eyes
HP1 RNAi	3	*w[1118];P{w[+mC]=CG8409*	Orange eyes
ptc-GAL4	2	*w[*]; P{w[+mW.hs]=GawB}ptc[559.1]*	Orange eyes
HP1RNAi, Csk RNAi	3	*w[1118];P{w[+mC]=CG42317,P{w[+mC]=CG8409*	Red eyes
ptc-GAL4, UAS-GFP	2,2	*w[*]; P{w[+mW.hs]=GawB}ptc[559.1], P{w+mC=UAS-2xEGFP}AH2*	Red eyes
DmHP1 (OE)	3	y[1] w[67c23]; P{y[+t7.7]=CaryP}attP2,HP1(OE). Insert into P2(3L) 68A4	Red eyes
kd, DmHP1OE	3	y[1] w[67c23]; P{y[+t7.7]=CaryP}attP2, HP1 (OE). Insert into P2:(3L) 68A4, Csk RNAi P{w[+mC]=CG42317	Red eyes
HP1kd,DmHP1OE	3	y[1] w[67c23]; P{y[+t7.7]=CaryP}attP2, HP1 (OE). Insert into P2:(3L) 68A4; HP1 RNAi P{w[+mC]=CG8409	Red eyes
Csk1 kd, HP1 kd, DmHP1OE	3	y[1] w[67c23]; P{y[+t7.7]=CaryP}attP2, HP1 (OE). Insert into P2:(3L) 68A4, HP1 RNAi P{w[+mC]=CG8409, Csk RNAi P{w[+mC]=CG42317	Red eyes
hHP1α	3	y[1] w[67c23]; P{y[+t7.7]=CaryP}attP2, w[m+C]=UAS-hHP1α-FLAG	Red eyes
hHP1α, dmHP1 KD	3	y[1] w[67c23]; P{y[+t7.7]=CaryP}attP2, w[m+C]=UAS-hHP1α-FLAG, CG*409	Red eyes
hHP1α, Csk KD	3	y[1] w[67c23]; P{y[+t7.7]=CaryP}attP2, w[m+C]=UAS-hHP1α-FLAG, CG*409, Csk RNAi P{w[+mC]=CG42317	Red eyes
hHP1α, Csk KD, dmHP1 KD	3	y[1] w[67c23]; P{y[+t7.7]=CaryP}attP2, w[m+C]=UAS-hHP1α-FLAG, CG*409, Csk RNAi P{w[+mC]=CG42317, dmHP1 RNAi P{w[+mC]=CG8409	Red eyes

Table 2.1: Table of *Drosophila melanogaster* genotypes

2.5: Confocal microscopy

Confocal microscopy was carried out on a Leica SP5 DM6000B Confocal microscope. When

imaging wing imaginal discs, images requiring the entire disc were acquired using a 20x (NA 0.5) objective lens, while immunohistochemistry and invasion assay samples requiring focus on the A/P boundary compartment used an oil immersion 63x objective lens (NA 1.4) to visualise the boundary cells. Z-stack projections to capture cell location through the depth of the tissue were acquired by sequential imaging with 0.67µm offsets of the focal plane between the top and bottom of the imaginal disc.

Imaging of immunofluorescent cultured mammalian cells on coverslips used oil-immersion 63x objective lens (NA 1.4), with an additional 3x magnification to achieve an 82nm/pixel resolution. Cross-sectional images across the field of cells were collected with 0.35µm vertical offsets from the base to the apical region and used to generate a Z-stacks using maximum intensity projection.

Laser excitation wavelength, and collection ranges appropriate to the fluorophores of each sample were used to detect the emission spectra of the specific combination of DAPI (ex405n, em410-530nm), green fluorescent protein (GFP) (ex 408nm, em500-550nm) and the secondary antibody Alexa fluorophores; 488 (ex588nm, em520-555nm), 555 (ex555nm, em565-600nm) or 647 (ex647, em670- 720nm).

2.6: Quantification of cellular invasive potential in imaginal discs

Following dissection and mounting of imaginal discs of fly larvae for a particular genotype, a maximum Z-projection of the ptc-driven GFP fluorescence in the upper region of the A/P boundary was collected. The main stripe of fluorescent epithelial cells of the boundary compartment, and the smaller regions of invasion were then traced with selection tools in ImageJ (Abràmoff, Magalhães, & Ram, 2004), and saved to separate region of interest (RoI) layers. Tracing the outline of each region of cells was performed with reference to the individual image slices to increase accuracy and consistent differentiation of invasive and non-invasive cells along the A/P boundary. The total area of the boundary compartment and cumulative invasive area was then calculated by the ImageJ software, along with the Z-depth for each sample, and then exported to Microsoft Excel for further analysis and graphing. A p value <0.05 is considered to represent statistical significance.

2.7: Cloning the Human HP1α cDNA into the pUASTattB Plasmid

PCR was used to amplify Human HP1α from MCF7 cell cDNA previously collected in the laboratory, before it was ligated in the pUASTattB plasmid, from which it was used for PhiC31-mediated recombination into the genome of *Drosophila* embryos.

The KAPA HiFi HotStart PCR Kit (KK2601) was used to amplify human HP1α with additional 3' EcoRI restriction site, 5' FLAG tag and 5' XhoI restriction site. Each primer was used at a concentration of 0.3µM.

Forward Primer:

FhHP1a EcoRI For: A TAA **GAA TTC** ATG GGA AAG AAA ACC AAG CG (30 bp)

Reverse Primer:

RhHP1a XhoI FLAG Rev: A TCC **CTC GAG** TTA CTT GTC GTC ATC GTC TTT GTA GTC GCT CTT TGC TGT TTC TTT CTC (58 bp)

Insert Map: EcoRI – human HP1α – FLAG – XhoI

Product: 620 bp

Optimisation of the PCR protocol was required as annealing temperatures over a 20ºC range showed very little product produced, at the correct 620bp size at 58.5ºC. This was due to the larger reverse primer containing the additional FLAG tag, requiring a much higher annealing temperature. A two-step PCR protocol was optimised to allow a low temperature annealing of primers to DNA for five cycles, before a further 25 cycles, annealing at 60-70ºC (Figure 5B). The two-step PCR protocol, with 70ºC annealing step following an initial five cycles to allow partial binding of primers to cDNA was used to generate the hHP1α-FLAG insert.

PCR Program

- 95°C 3 minutes
- 98°C 20 seconds
- 53ºC 15 seconds
- 72°C 30 seconds

} 10 cycles

- 98°C 20 seconds
- 70ºC 15 seconds
- 72°C 30 seconds

} 20 cycles

- 72°C 1 minute
- 4°C HOLD

Six replicates of this PCR reaction were produced, purified using ChargeSwitch Pro PCR Clean-up Kit, and run on a 1% Agarose Gel. Under UV light, the 620bp hHP1α-FLAG band was cut from the gel to separate it from primers and purified using a PureLink Quick Gel Extraction Kit.

The pUASTattB plasmid stock available in the laboratory already contained the dmHP1FLAG gene at the same restriction site required for the new insert, which required cutting out the ~660bp band and gel purifying the remaining plasmid. The vector double digests were run on 1% agarose, and gel purified, cutting out the 660bp insert and saving the 8489bp plasmid band.

The pUASTattB- DmHP1FLAG vector and hHP1α-FLAG DNA were simultaneously double-digested with both EcoRI and XhoI to prepare for insertion of hHP1α-FLAG PCR product. Single digest controls of the pUASTattB-DmHP1FLAG plasmid were performed to check both enzymes cut as expected and run on a 1% agar gel (Figure 13A). Equivalent of 5U of each enzyme was used in each digest. Double digest of the pUASTattB-DmHP1FLAG shows the 660bp band associated with the *Drosophila* HP1-FLAG DNA, while the double digests of the insert DNA show the correct 620bp position for the human HP1α-FLAG insert. The vector band shows a concentration of 80ng/µl, while insert is estimated to be 8ng/µl.

Purified pUASTattB plasmid vector was treated with Rapid alkaline phosphatase (Roche; 04898133001) following manufacturer's directions, before a ligation series was set up with increasing ratios of insert to vector DNA from 1:1, 1:3 and 1:5. Plasmids were ligated using 1U NEB T4 DNA Ligase per 20µl reaction.

DH5α competent cells (Invitrogen) were used for optimum transformation efficiency. The cells were resuspended in 50ul aliquots with 4ul of each ligation and incubated on ice for 30 minutes, before being incubated at 42ºC for 45 seconds. 500µl of SOC medium (Sigma-Aldrich) was added to each tube, and samples were incubated for one hour at 37ºC. Cells were centrifuged and resuspended before being plated on LB agar + Ampicillin (100µg/mL) plates overnight at 37ºC.

Using an Intron Mini prep kit, following manufacturer's directions, DNA was isolated from

transformed DH5α colonies that exhibited ampicillin resistance due to the pUASTattB plasmid, and quantified on a NanoDrop. A double digest with EcoRI and XhoI was set up to identify any colonies successfully transformed with the insert, which were identifiable as the ~620 bp band observed in colonies one and two exhibited the insert.

2.8: Maintenance of MCF7 Cell lines

MCF7 (ATCC) cell lines, both control and constitutive HP1α KD, were maintained in DMEM (Gibco) with 1% penicillin/streptomycin (Gibco), 10% fetal bovine serum (FBS) (Gibco), ten g/mL insulin (Sigma-Aldrich) and 35 g/mL hygromycin B (Gibco) at 37C with 5% CO_2 in a humidified incubator.

Cells were passaged every three days as they reached confluent growth in 75 cm^2 corning flasks in 20 mL of supplemented DMEM media, up to a maximum of 25 passages, after which fresh cells were grown from -80ºC frozen stocks. To passage, old growth media was removed, and cells washed twice in a phosphate buffered saline (PBS) (Gibco), before adding 1.5mL of 0.25% Trypsin-EDTA (Gibco) for 4-5 minutes to allow detachment of cells from the surface of the flask. DMEM was added to bring the volume of 10mL to inactivate the trypsin and resuspended vigorously to achieve a single cell suspension. An appropriate percentage of total cells- typically 30% for control and 40% for HP1α KD were made up to 20mL volume in DMEM in a fresh flask to continue the culture, while the remaining cells were used in experiments.

2.9: Applying mechanical shear force to MCF7 Cells

MCF7 cells of both control and HP1α KD at confluence were harvested via trypsin treatment and resuspended in 1x PBS to a final concentration of $1x10^6$ cells/mL. 1mL of suspension was immediately aliquoted into a 1.5mL centrifuge tube, with 10µl removed and loaded on to a prepared haemocytometer for imaging. Using a 1mL syringe, cells were passed through a 26G (0.26mm inner diameter) needle at a rate of five passages per minute, and every specified passage number an aliquot was taken for counting and the control and HP1α KD tubes for passaging alternated.

The haemocytometers were imaged on a light microscope at 100x magnification with fine focus on the gridlines, and four fields of view were captured. Whole cells and free nuclei were

visually distinguished, as were nuclei from cellular debris as shown in Figure 5. Manual counts of whole nuclei were made and averaged across the number of passage cycles. Whole cells were counted as intact nuclei in the 0x samples, and very few whole cells remained following 10x passages, indicating an equivalent of rate breakdown of the outer membrane and release of nuclei for both cell types, which is consistent with rates of breakdown in the literature, which show loss of cellular membrane after as few as two passages (Furusawa et al., 2015).

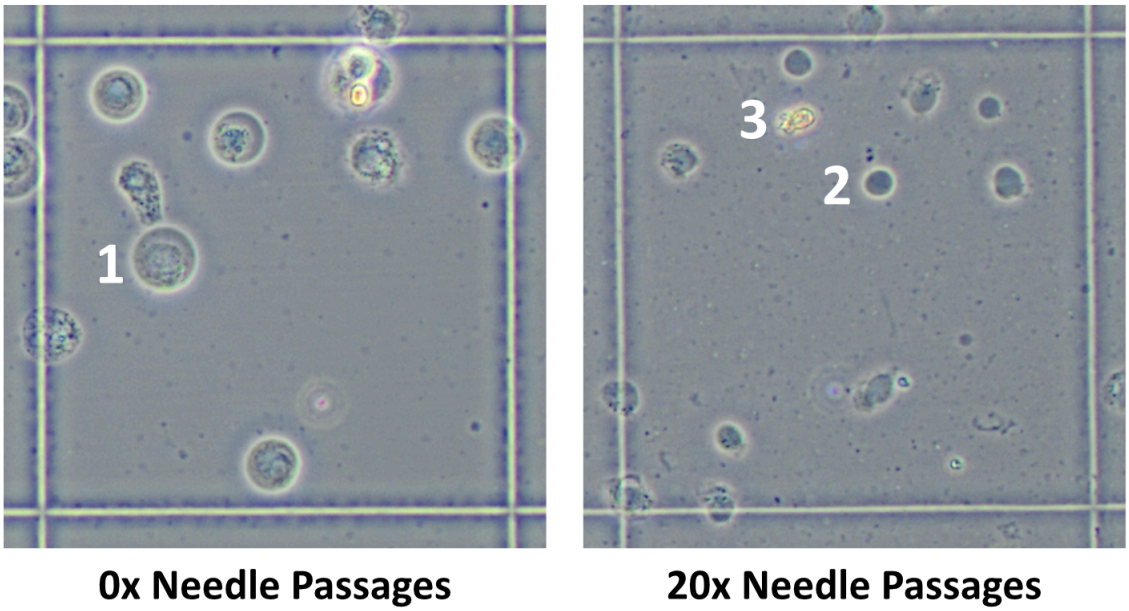

Figure 5: Representative image of MCF7 control cells before and after exposure to mechanical shear force, showing release of nuclei from whole cells.
1) Whole intact cell. 2) Released whole nuclei. 3) Cellular debris. Grid square corresponds to 250x250μm.

During the optimisation of this assay, the experiment was initially performed by two people, so that the nuclei could be counted in real time as haemocytometers were loaded with fresh aliquots following a passage set. However, this method proved impractical due to the large number of samples involved. Imaging all the prepared haemocytometers after the syringing was finished proved far more consistent and accurate. To ensure results would not be impacted by degradation or drying of cells, test samples were imaged and compared over a 40-minute timeframe- well in excess of the time required for sample preparation- and no changes were observed.

2.10: MCF7 cell fractionation

Asynchronously growing MCF7 control and HP1α KD cells were harvested at confluence via trypsin treatment. The cell suspension was diluted to approximately $1x10^6$ cells/mL to enable

accurate cell counting on haemocytometer to calculate actual concentration. Equal numbers of cell type were removed, with a minimum of $5x10^6$ cells. The cells were then washed in PBS, and resuspended in Kapoor Buffer A (20 mM Tris-HCl pH 7.5, 75 mM KCl, 30 mM $MgCl_2$, 1 mM DTT, 0.5 mM EDTA, 0.5% NP40, cOmplete EDTA-free protease inhibitor) to a concentration of 0.5 x 10^6 cells/100 µl, and incubated on ice for ten minutes with intermittent vortexing. Half of the sample volume was removed and retained as the whole cell lysate fraction. The remaining sample was centrifuged at 7000 x *g* for ten minutes at 4°C, before removing supernatant and retaining as the cytoplasmic fraction. The remaining pellet was resuspended in Kapoor Buffer A in same volume of removed supernatant, to provide the nuclear fraction. Lysates were stored at -80ºC, and heat treated with SDS laemmli dye prior to loading on SDS-PAGE gel.

2.11: Nuclear envelope isolation

A minimum of 20 $x10^6$ asynchronously growing MCF7 control and HP1α KD cells were harvested at confluence, diluted appropriately for accurate cell counting on the haemocytometer, washed in PBS and resuspended to a concentration of $1x10^6$ cells/mL. The cells were counted again before, removing equal cell numbers of at least 20 x 10^6 cells and centrifuged at 200x g for 5min, before removing PBS.

The Nuclear Envelope Protein Extraction Kit (101Bio; P513L) was used, following manufacturer's instructions. Cells were resuspended in 1mL cold PBS and pellet in a centrifuge tube at 200 x *g* for five minutes at 4ºC. The supernatant was removed, and the pellet resuspended in 500µl of the Buffer A lysis solution supplied with the extraction kit. The cells were incubated on ice for ten minutes before being vortexed vigorously. The solution was transferred to a precooled filter cartridge and centrifuged at 18,000 x *g* for one minute. The filter was discarded, and the supernatant removed. The pellet was washed in cold PBS, then 300µl of the nuclear lysis Buffer B- supplied with the extraction kit- was added and incubated on ice for ten minutes with intermittent vigorous vortexing. The samples were centrifuged at 6,200 x *g* and the supernatant transferred to a fresh tube, adding 800µl cold PBS and inverting repeatedly to precipitate nuclear envelope. The envelope was pelleted at 18,800 x *g* for 15 minutes at 4ºC, before the supernatant was removed and the remaining isolated nuclear envelope pellet was resuspended in 1x SDS PAGE dye, and heat. Samples were stored at -80ºC prior to loading on an SDS-PAGE gel.

2.12: Immunoblotting

Protein samples were pre-treated by reducing and denaturation agents in 1x laemmli buffer and heated to 99ºC for 5-10 minutes. An SDS-PAGE gel was poured and set in a Bio-Rad SDS-PAGE apparatus following manufacturer's instructions. The acrylamide concentration was determined by the molecular weight of intended protein target, a 10% acrylamide gel was used for A-type lamins which have molecular weights between 65 and 73 kDa, and 12% was used when blotting for core histone proteins, to provide better resolution of much smaller molecular weights. Once the gel was set and apparatus filled with running buffer (25 mM Tris, 192 mM Glycine, 1% SDS) the protein samples were loaded along with PageRuler size markers. The gel was run at 30V for 30 minutes to allow samples to enter the stacking gel, before voltage was increased to 130V and run until the dye front reached bottom of the gel. Once finished, the gel was removed from the apparatus and glass plates, and the stacking gel and dye front were removed. The gel was transferred onto a 0.1µm nitrocellulose membrane that had been soaked in pre-chilled transfer buffer and sandwiched between three sheets of cartridge paper on either side inside the transfer cassette. The cassette was then loaded into a Bio-Rad transfer apparatus and the transfer run at 100V for 60 minutes at 4ºC with constant stirring. Once complete the membrane was removed from the gel and cassette, then trimmed to a convenient size for staining. When optimising a western blot protocol, reversible Ponceau staining (Sigma Aldrich #78376) of the membranes was used to check the transfer was successful, as well as to visually compare total protein bands present on the membrane.

The membrane was then blocked in 5% skim milk in wash buffer (20 mM Tris, 150 mM NaCl, 0.1% Tween 20) for one hour, before being incubated in the appropriate primary antibody, diluted in blocking buffer, overnight. Following primary incubation, the membrane was rinsed in in wash buffer, then washed twice for five minutes and then twice for 10 minutes in the same buffer. The membrane was then incubated with the secondary HRP antibody for one hour, before the washing steps were repeated and the blot was developed using ECL reagent (GE healthcare) following manufacturer's instructions and visualised using an Azure Biosystems cSeries Gel doc.

2.13: Isolation of whole nuclei from MCF7 Control and HP1α KD cells

Asynchronously growing MCF7 control and HP1α KD cells were harvested at confluence as described in Section 2.8 and counted. Equal numbers of at least $6x10^6$ cells for each cell type

were removed for nuclei extraction and washed with cold PBS so cells are at a concentration of 1 x 10^6/mL. The cell suspension was then recounted, and after a second wash, 5x10^6 cells were removed. The cells were resuspended in cold nuclei extraction buffer (320 mM sucrose, 10 mM HEPES, 5mM $MgCl_2$, 1% Triton X-100) at a concentration of 1 x 10^6 cells/mL, and vortexed gently for 10 seconds. The cells were incubated on ice for 15 minutes to allow lysis of the cytoplasmic membrane, vortex mixing every five minutes, before the nuclei were pelleted at 2000 x *g* for five minutes. The nuclei were washed with nuclear wash buffer (320 mM sucrose, 10 mM HEPES, 5mM $MgCl_2$), and stored on ice.

2.14: Immunostaining of whole of MCF7 cells

Acid-etched Poly-D-Lysine coverslips were prepared by incubating five mm glass coverslips in 1M HCl overnight at 60ºC, before washing and treating with Poly-D-Lysine for one hour. Slides were washed in ddH20, dried and UV-treated before being stored. Acid etching of the coverslips roughens the glass to enable better attachment of cells as well as the poly-amino acids, which themselves aid cell attachment to the surface.

Asynchronously growing MCF7 control and HP1α KD cells were harvested and were used to seed two coverslips in each well of a 24 well plate (SIGMA #CLS3527), one well for each antibody condition to be tested. Wells were seeded at a concentration of ~3x10^5 cells/well/2mL and incubated at 37ºC with 5% CO_2 for three days. The coverslips were washed twice with PBS with $MgCl_2$ and $CaCl_2$ and fixed in 4% paraformaldehyde for 15 minutes at room temperature, followed by permeabilization in PBS + 0.2% Triton X-100 for five minutes at room temperature. The coverslips were then blocked for 30 minutes in PBS+5% bovine serum albumin (BSA) + 0.5% Tween-20 for 30 minutes, rocking at room temperature.

Primary antibodies (See Table 2.2) were diluted in PBS+5% BSA + 0.5% Tween-20, and cover slips in the wells were incubated overnight while rocking in their respective antibody at 4ºC. Samples were washed three times for five minutes on an orbital shaker, and then incubated with the appropriate Alexa fluorophore secondary antibody, rocking for one hour at room temperature.

The coverslips were washed again, then post fixed in 2% paraformaldehyde for 15 minutes at room temperature, before being counterstained with 300 µl of DAPI (300 mM) per well. The coverslips were then removed from the wells, rinsed in ddH_2O, and mounted in SlowFade

(Thermo Fisher #S36937). Samples were imaged on a confocal microscope as described in Section: Confocal Microscopy.

2.15: Protein solubility assay from whole nuclei

Whole nuclei were isolated from MCF7 control or HP1α cells as described in Section 2.8. The clean nuclei pellet was then resuspended in 300µl of ice-cold salt extraction buffer (10 mM Tris pH 7.4, 2mM $MgCl_2$, 0.1%Triton X-100, 1mM DTT, cOmplete EDTA-free protease inhibitor, and NaCl concentrations: 50 mM, 150 mM, 250 mM, 500 mM) starting with lowest NaCl concentration (50 mM). The resuspended pellet was incubated for 15 minutes at 4ºC with gentle nutating. The insoluble material was pelleted for 10 minutes at 2000 x *g* at 4˚C. The supernatant was completely removed and labelled as the 50 mM NaCl sample. The extractions were repeated with increasing NaCl concentration for both control and HP1α KD cells, for a complete set of 50 mM, 150 mM, 250 mM and 500 mM salt extracts. The protein extracts were denatured, and heat treated with 1x laemmli buffer, and stored at -80ºC.

2.16: Preparation of MCF7 cells for electron microscopy

Processing of samples was performed by the Manawatu Microscopy and Imaging Centre.

Samples trimmed to the correct size and shape were fixed in Modified Karnovsky's Fixative (3% Gluteraldehyde (Merck) (v/v) 2% Formaldehyde (w/v) in 0.1M Phosphate Buffer (pH7.2)) for at least two hours. The samples were washed in 0.1M phosphate buffer (pH7.2) three times for 10 minutes each, followed by post-fixing in 1% Osmium Tetroxide in 0.1M phosphate buffer for one hour maximum. The sample was then buffer washed as above three times for 10 minutes each, followed by dehydration through a graded acetone series (25%, 50%, 75%, 95%, 100%) for 10-15 minutes each followed by two changes of 100% acetone for one hour each.

Samples were then put into 50:50 resin:acetone and placed on the stirrer overnight
This was replaced by fresh 100% resin (Procure 812, ProSciTech Australia) for 8 hours on the stirrer. This step was repeated twice more (overnight in 100% resin, 8 hours in 100% resin)
Samples were embedded in moulds with fresh resin and cured in a 60˚C oven for 48 hours.

Light microscope sections were cut at one micron using a glass knife on the ultramicrotome (Leica EM UC7, Germany) and heat fixed onto glass slides. These were stained with 0.05% Toluidine Blue for approximately 12 seconds and viewed under the light microscope
The block was then trimmed down to the selected area and cut using a Diamond Knife (Diatome, Switzerland) at 100nm (light gold sections). These were stretched with chloroform vapour and mounted on a grid using a Quick Coat G pen (Daido Sangyo, Japan).

The grids were stained in Saturated Uranyl Acetate in 50% Ethanol for four minutes, washed with 50% ethanol and MilliQ water and then stained in Lead Citrate (Venable and Coggeshall, 1965) for a further four minutes. This was followed by a wash in MilliQ water
Samples were viewed using a an FEI Tecnai G^2 Spirit BioTWIN (Czech Republic).

2.17: Sample preparation for mass spectroscopy

For identification of discrete protein bands by mass spectrometry, the protein samples were first resolved by SDS PAGE. The acrylamide gel was incubated for 30 minutes in fixative (40% MeOH, 10% acetic acid, in deionised water), and washed twice in deionised water for 10 minutes. The gel was stained with colloidal Coomassie blue G-250 (Thermofisher) overnight, and de-stained in deionised water.

Protein bands of interest were excised from the gel inside a HEPA filtered laminar flow hood, diced very fine, and transferred to 1.5mL Eppendorf LoBind tubes. The gel fragments were de-stained in ammonium bicarbonate solution (50mM ammonium bicarbonate pH 7.9) (ABC), and the solution was refreshed regularly over two hours until colourless. The gel fragments were then dehydrated in 80% acetonitrile for one minute and dried completely using a centrifugal evaporator.

The fragments were then incubated in a reducing buffer (10mM DTT in ABC) for one hour at 37ºC and washed in ABC before dehydration in 80% acetonitrile. In the dark, the samples were incubated at room temperature for 30 minutes in an alkylation buffer (20mM iodoacetamide in ABC), before they were washed and dehydrated twice with ABC and 80% acetonitrile, then dried with centrifugal evaporation. The gel pieces were then incubated in a digestion solution (20ng/µl trypsin in ABC) overnight at 37ºC, before sonicating for two

minutes in an ultrasonic bath, and the supernatant was collected. For each sample, the supernatant was pooled with subsequent washes and sonication of the gel fragments, firstly with 5% formic acid in 50% acetonitrile, then 0.1% formic acid in 80% acetonitrile. The total volume of the extracted protein for each of the band samples was reduced to ~30µl by centrifugal evaporation, and mass spectroscopy was carried out by Trevor Loo, School of Fundamental Sciences, Massey University.

2.18: Table of antibodies

Name	Target	Host	Mono/ Polyclonal	Company	Catalogue #	Dilution used
Primary Antibodies						
Anti- dmHP1	*Drosophila* Su(var)205	Mouse	Monoclonal	Developmental Studies Hybridoma Bank	C1A9	1:50
Anti-FLAG	FLAG	Rabbit	Monoclonal	Sigma-Aldrich	F7425	1:50
Anti-Lamin A + C	Human	Rabbit	Monoclonal	Abcam	ab108595	1:500
Anti-Histone H3 [phosSer10]	H3 pS10	Rabbit	Polyclonal	ROCKLAND	600-401-I74	1:500
Anti-Lamin B Receptor	Human	Rabbit	Polyclonal	Thermo Fisher	PA5-66473	1:1000
Anti-Lamin B2	Mouse, Rat, Human	Rabbit	Monoclonal	Abcam	ab151735	1:1000
Anti-Lamin B1	Mouse, Rat, Human	Rabbit	Monoclonal	Abcam	ab133741	1µg/mL
Anti-Emerin	Mouse, Rat, Human	Rabbit	Monoclonal	Abcam	Ab156871	1:250
Anti-HP1α	Human, Mouse, Rat, Monkey	Rabbit	Polyclonal	Cell Signal	2616S	1:1000
Anti-PRR14	Mouse, Rat, Human	Rabbit	Polyclonal	Abcam	abb174532	1:200
Anti-BAF	Mouse, Rat, Human	Rabbit	Monoclonal	Abcam	ab129184	1:200
Secondary Antibodies						
Alexa 555	All Rabbit Ig's	Goat	Polyclonal	Invitrogen	A-21428	1:500
Alexa 647	All Rabbit Ig's	Goat	Polyclonal	Invitrogen	A-21236	1:500
Anti-Rabbit IgG-10nm Gold bead	All Rabbit Ig's	Goat	Polyclonal	Merck/Sigma Aldrich	G7402	1:100

Table 2.2: Table of antibodies for western blotting and immunofluorescence of cultured mammalian cells.

Chapter 3: Heterochromatin Protein 1 supresses malignant cell invasion in vivo

3.1: Introduction

3.1.1: *Drosophila melanogaster* model of epithelial cell invasion

Prior research in the laboratory indicates that loss of human HP1α is correlated with increased invasive potential in cultured cells with existing malignant pathways activated. However, in tumours, malignant cell invasion takes place in a complex tissue microenvironment where cancerous cells abut and infiltrate neighbouring cells in all directions in a manner that cannot be replicated in a cell culture environment.

In order to visualise and quantify invasive behaviour in response to HP1α modulation in a more applicable environment, a *Drosophila melanogaster* model was established previously in the laboratory (Solomon, 2016), based on the work by Vidal, Larson, and Cagan (2006). This assay measures the degree of epithelial cell invasion in the fruit fly larvae containing knocked-down expression of the fly HP1α homologue. The genomic structure of the HP1 family is conserved between *Drosophila* and humans. *Drosophila* contain the Su(var)205 gene that is homologous to the human CBX5 gene that encodes the HP1α protein. These genes share the same five exons and four intron structure, and the Su(var)205 translated protein, referred henceforth as dmHP1, has been shown to have functional similarity with the human homologue. Human HP1α is able to rescue lethality of homozygous mutants of dmHP1 (Norwood et al., 2004) providing evidence of a high degree of biological similarity between fly and human HP1α proteins, and that this model is of relevance to exploring human biochemistry.

This cellular invasion assay was first developed by Vidal et al. (2006) to measure the effect of selectively expressed and knocked-down genes of interest within a stripe of epithelial cells within the Anterior/Posterior boundary compartment of the wing imaginal disc of third instar larvae. This enables fluorescent visualisation of a discrete region of epithelial cells with specific gene modulation, within a field of wild-type cells. Any invasive characteristics these cells exhibit during larval growth, up to the point of dissection, can be observed (Figure 6). This technique utilises the GAL4/UAS gene expression system developed by Ornitz, Moreadith, and Leder (1991), which fuses the yeast transcriptional factor GAL4 downstream of a tissue-specific promoter, in this case *Patched (Ptc*). *Ptc* is a developmental gene that has

highly specific expression along the A/P boundary in *Drosophila* larvae. In order to regulate gene expression via *Ptc* promoter activation, the gene or RNAi of interest is fused downstream of the GAL4 Upstream Activating Sequence (UAS), which upon binding GAL4 induces transcription. In this manner, in tissues where the Ptc promoter is active, GAL4 is expressed, which in turn binds UAS and induces transcription of the linked gene in the same cell (Figure 7).

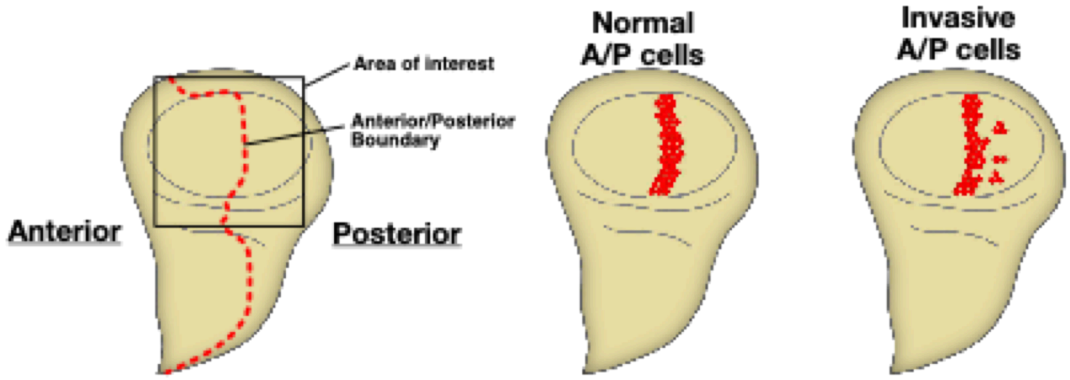

Figure 6: Illustration of third-instar larvae imaginal discs, visualising invasion of epithelial cells away from the A/P boundary during an invasion assay.

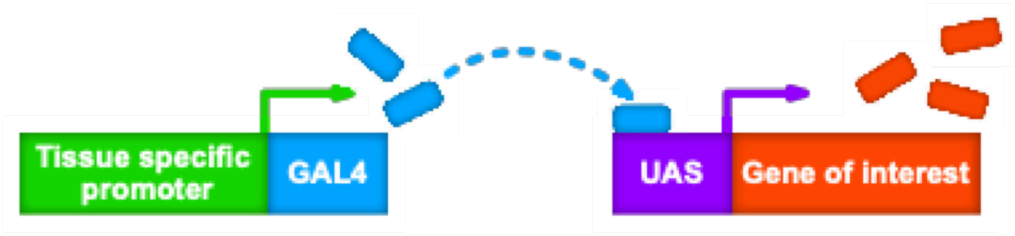

Figure 7: Diagram of GAL4/UAS controlled tissue-specific gene expression.
Activation of a tissue specific promoter allows transcription and translation of the downstream GAL4 gene, which as a protein can transcriptionally activate an Upstream Activating Sequence (UAS) not found natively in *Drosophila.* Activation of this region allows transcription of the downstream gene and enables co-localisation with the tissue specific promoter.

Vidal et al. (2006) used a KD of the C-terminal Src Kinase (Csk) protein, an inhibitor of the Src signalling pathway, to promote invasion. Src is a proto-oncoprotein that activates a cascade of pro-growth factors and is inactivated by phosphorylation by Csk (Figure 8).

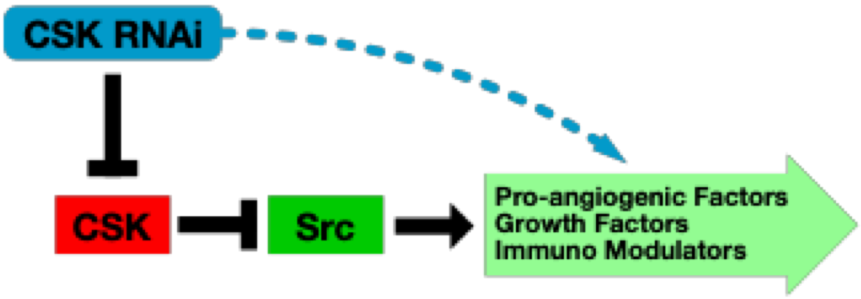

Figure 8: Activation of the Src malignant pathway following KD of the Csk protein
The Csk protein phosphorylates the Src oncoprotein, inhibiting its activity and promotion malignant pathways. When Csk interfering, RNA is expressed it binds to Csk mRNA, preventing translation and reducing Csk expression. This KD of Csk effectively activates the Src protein, as the inhibitory phosphorylation is not maintained, and malignant pathways are activated.

3.1.2: dmHP1 over-expression supresses Src pathway driven cell invasion

Previous work in the laboratory (unpublished) established a synergistic relationship between dmHP1 KD and Src activation driving cellular invasion, by coupling a Csk-KD genotype with a dmHP1 KD, and showing a significant increase in the degree of epithelial invasion beyond the anterior/posterior boundary of the GFP demarcated imaginal disk, compared to Src pathway activation alone (Figure 9).

Invasiveness was compared between the control line containing only Ptc-GAL4 driven GFP fluorescence, the Csk KD line as cells containing a malignant pathway, dmHP1 KD line as non-malignant cells with reduced dmHP1 expression, and a double KD of dmHP1 and Csk as a model of dmHP1 loss in cells with existing malignancy activation.

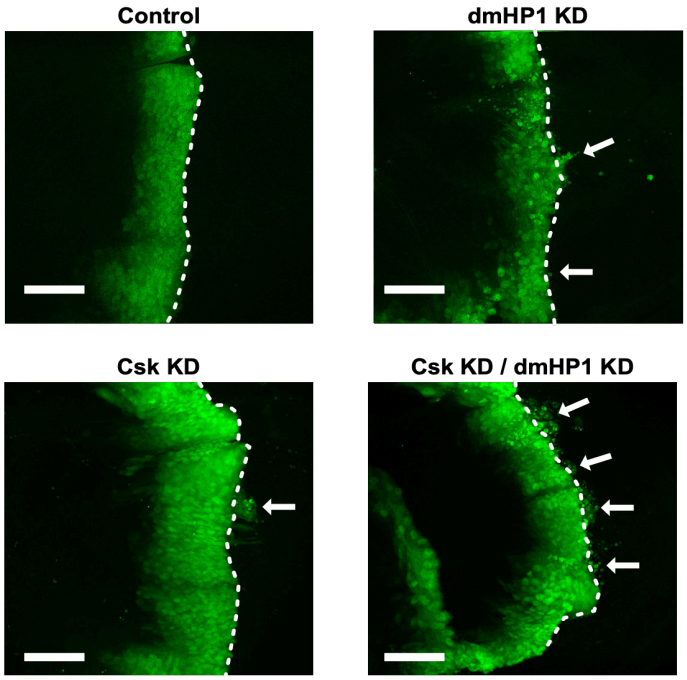

Figure 9: Representative confocal Z-projections imaginal disks demonstrating activation of Src synergistically enhances cell invasion of A/P epithelial cells.
Dotted line represents posterior edge of A/P boundary, and arrows indicate regions of cellular invasion. Images taken at 630x magnification with 0.67μm increments, with 8-15 samples per construct. Scale bar = 50μm. Figure adapted from my Honours Research Report (Solomon, 2016).

3.2: Results

3.2.1: DmHP1 overexpression rescues Src activated invasive phenotypes in vivo

To confirm that it is dmHP1 KD that promotes invasion rather than an off-target effect, dmHP1 was reintroduced to determine whether it could rescue the invasive phenotype. Dr Helen Fitzsimons (School of Fundamental Sciences, Massey University, New Zealand) provided a *Drosophila* line (DmHP1 OE) with a UAS-linked *Drosophila* FLAG-tagged dmHP1 gene. Firstly, this line was crossed with the *Ptc*-GAL4/UAS-GFP flies to confirm that DmHP1 was expressed. Third instar larvae of the progeny were dissected to collect the imaginal discs, and immunohistochemistry (Section 2.3) was performed using FLAG antibody to detect FLAG-HP1 expression. No FLAG protein was detected in negative control discs (Figure 10A) containing only the *Ptc*-GAL4/UAS-GFP gene, and successful expression of the dmHP1-FLAG protein was detected along the A/P boundary line (Figure 10B). There was a punctate sub-cellular distribution of dmHP1-FLAG in the nucleus as expected. As the staining procedure for the imaginal disks requires rotating the tissue in an antibody solution overnight, the delicate imaginal disc organelles are easily damaged and torn. This means that samples following the staining procedure are often stretched or disfigured and are not representative of the larvae used for the assessment of invasion (Figure 10).

To assess whether expression of dmHP1 rescued the dmHP1 KD phenotype. The UAS-dmHP1-FLAG line was crossed with fly lines containing either the CSK KD RNAi line to provide an active Src pathway, dmHP1 KD RNAi, or both dmHP1 KD and the CSK RNAi. The imaginal discs were dissected from progeny of these crosses at the third instar larval stage and immunohistochemistry performed with a FLAG antibody to visualise dmHP1-FLAG expression and localisation (Figure 10C-E). Imaginal discs of larvae with the dmHP1 KD/dmHP1 OE genotype showed decreased expression compared to the control larvae, as the RNAi also targets the dmHP1-FLAG mRNA. While the Csk KD/dmHP1 OE and Csk KD/dmHP1 KD/dmHP1 OE genotypes display increased levels of dmHP1 along the A/P boundary when compared to the control, indicating successful over-expression.

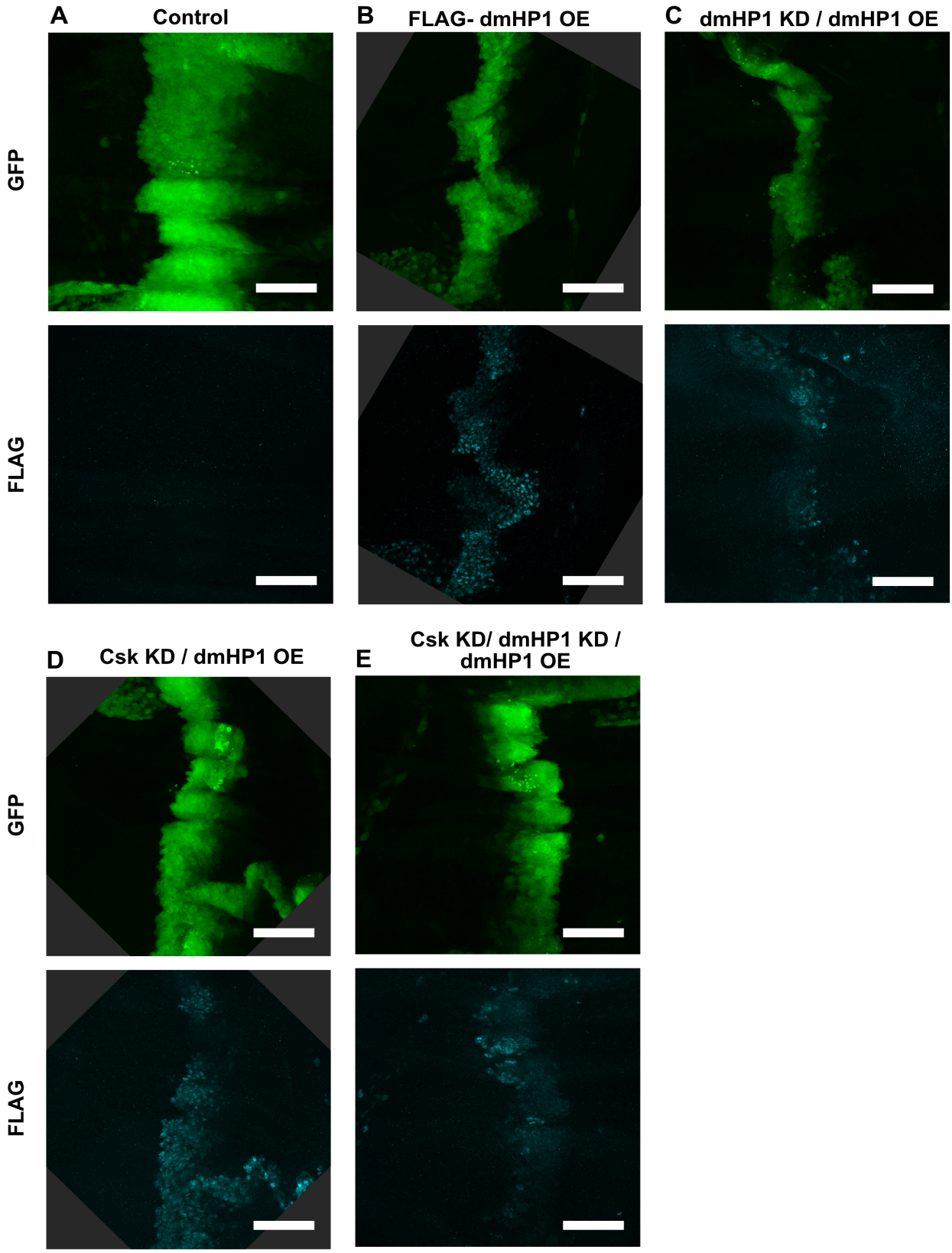

Figure 10: Immunohistochemistry staining for the presence of FLAG-tagged HP1 over-expression along the A/P boundary.
Maximum intensity z-stack projections of third instar *Drosophila* larvae that were processed for immunohistochemistry, using Rabbit anti-FLAG (Sigma F7425) primary antibody to detect FLAG-tagged dHP1. Alexa Fluor® 647-conjugated goat anti-rabbit IgG was used as the secondary antibody

at 1/500 dilution. Confocal z-stack was collected over the height of the disc at 630x magnification. Scale bar = 50μm.

To identify the effect of over-expression on invasion, third instar larvae of the genotypes shown in Figure 10 were harvested (Section 2.6) in order to quantify the total area of invasive cells that invade beyond the distinct boundary on the posterior side of the A/P boundary line in the imaginal disc. The z-stack image data was quantified for each genotype construct across multiple biological replicates and graphed in Figure 12. The control line contains only the Ptc regulated GFP expression, which causes fluorescence along the A/P boundary of the imaginal discs. These control larvae showed consistent and well-defined posterior edge boundaries, with no indication of cell migration beyond the discrete posterior boundary (Figure 11A). Knock down of the dmHP1 over-expression larvae (Figure 11C) exhibits a small increase in cell migration, to roughly the same extent as the KD of dmHP1 in addition to the dmHP1 over-expression in Figure 11D. The degree of invasion following over-expression of dmHP1 for both 11C and 11D is less than 11B, indicating the presence of the additional dmHP1 gene is able to compensate for the KD, and restrains invasive activity to a level close to the control flies (Figure 11A).

The effect of dmHP1 over-expression was then tested in flies with a malignant pathway activation, due to Csk KD. Previous work had shown a strong synergistic interaction between loss of dmHP1 and activation of Src, which resulted in a seven-fold increase in invasive behaviour, compared to Csk KD alone (Figure 11G and I). Over-expression of dmHP1 in addition to the double KD, rescued the invasive phenotype of the flies, reducing invasive behaviour to near the equivalent level of the Csk KD genotype flies (Figure 11J). The significant increase in invasive behaviour was not observed in response to restored dmHP1, demonstrating dmHP1 is specifically required to modulate the effect. Excess dmHP1 further reduced the invasive phenotype of flies with reduced Csk expression (Figure 11I).

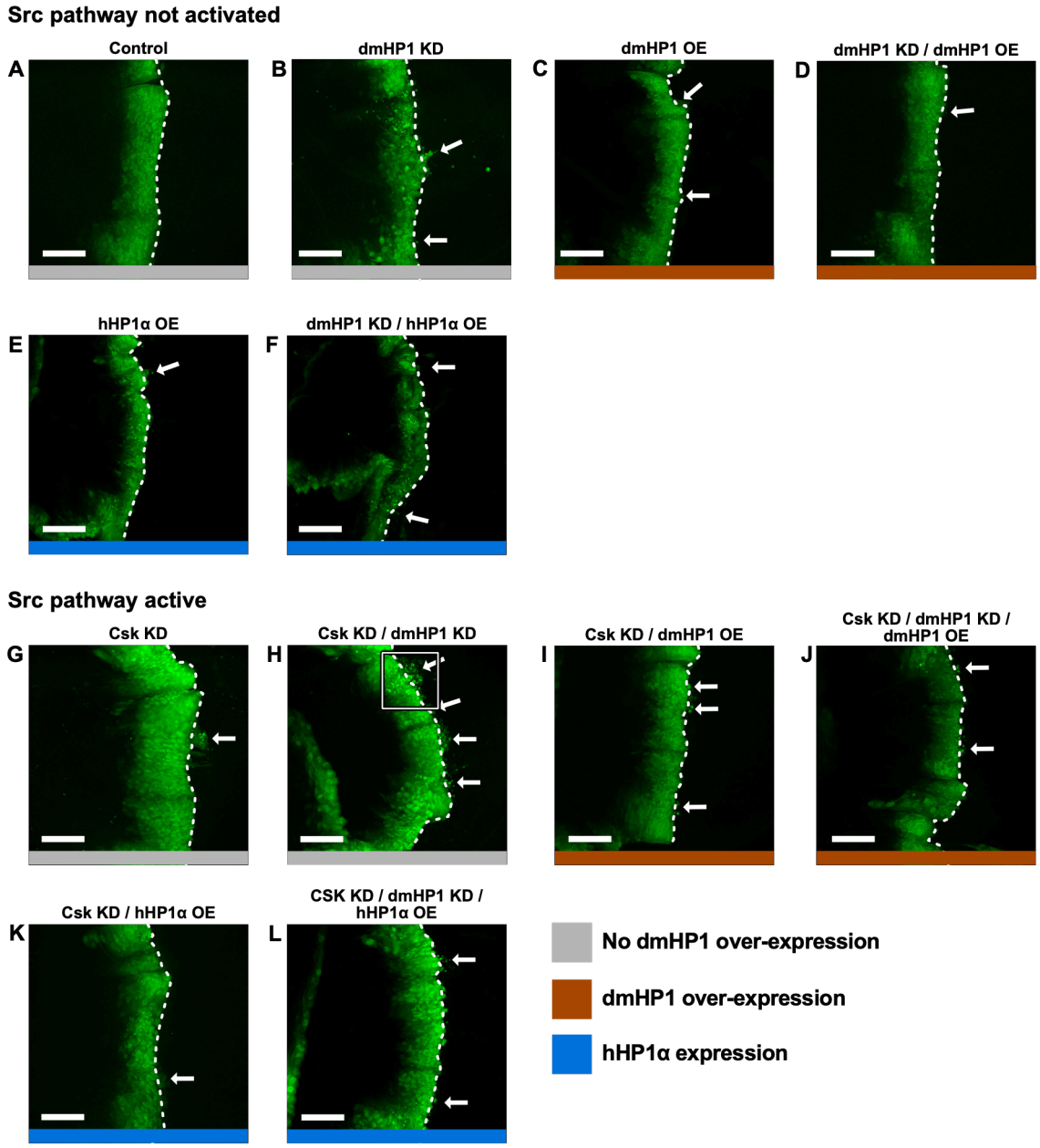

Figure 11: Representative images of the imaginal disc invasion assay
Representative confocal Z-projections of Ptc-driven GFP fluorescence along the A/P boundary of imaginal discs dissected from third instar larvae. Activated cancerous pathway indicates the presence of the Csk KD, which activates the Src onco-pathway. Larvae genotypes have either endogenous *Drosophila* HP1 (dHP1) or human HP1α (hHP1α), knocked down or over-expressed. The dotted line represents the posterior edge of A/P boundary, and arrows indicate regions of cellular invasion. Images taken at 630x magnification with 0.67μm z-height increments. Scale bar = 50μm. Samples A, B, G and H are sourced from data initially published as part of an honours report (Solomon, 2016).

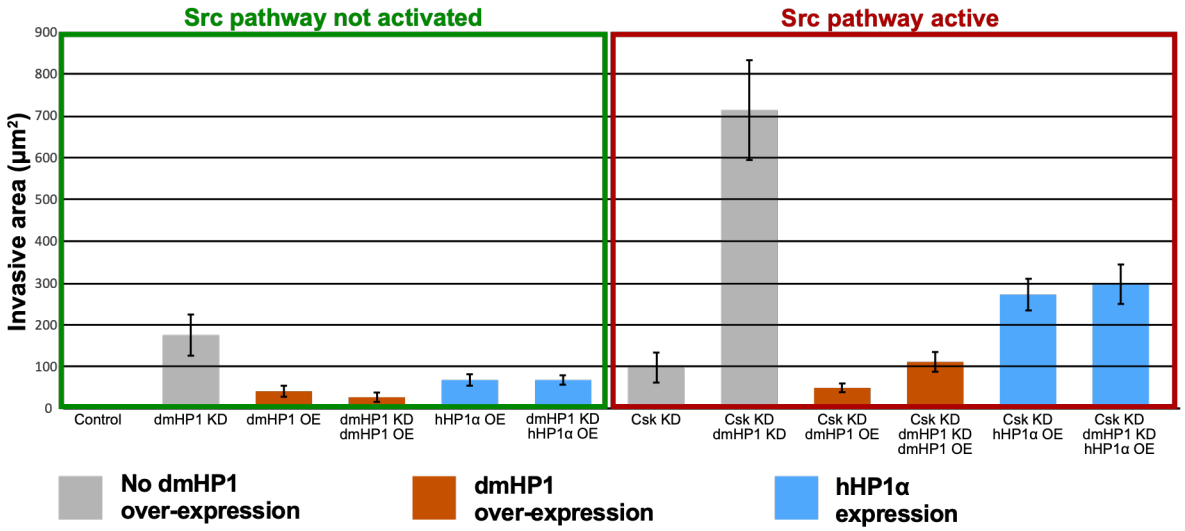

Figure 12: Graph of HP1 modulating of cellular invasiveness in *Drosophila* larval imaginal disks in conjunction with cancer pathway activation

Quantified levels of invasive phenotypes calculated by average area of invasion beyond the posterior edge of the imaginal disk A/P boundary. All lines contain the Ptc-GAL4/UAS-GFP genes to drive GFP fluorescence along the A/P boundary, in addition to labelled genotypes A) n= 11. B) n= 8. C) n= 11. D) n= 8. E) n= 11. F) n= 8. G) n= 14. H) n= 18. I) n= 16. J) n= 14. K) n= 14. L) n= 13. Samples A, B, G and H are sourced from data initially published in (Solomon, 2016).

3.2.2: Preventing invasion with expression of hHP1α

To determine whether *Drosophila* and human HP1α are of sufficient functional similarity to enable human HP1α (hHP1α) to rescue the invasive phenotype resulting from dmHP1 KD (Figure 11H), the human HP1α CBX5 gene was inserted into a *Drosophila* line, downstream of the UAS- containing promoter.

Firstly, the generation of this transgenic construct required cloning the hHP1α cDNA into the pUASTattB insertion vector. pUASTattB contains a multiple cloning site downstream of a UAS, an attB site for generation of transgenic flies via PhiC31-mediated recombination and the *white (w*) gene for eye colour based selection of transgenic progeny (Groth, Fish, Nusse, & Calos, 2004). The cloning to create the pUASTattB plasmid containing a FLAG-tagged hHP1α cDNA is described Section 2.1. The pUASTattB plasmid containing a dmHP1-FLAG had already been constructed. Digestion of this plasmid with XhoI and EcoRI released the DmHP1-FLAG, and FLAG-hHP1α was inserted into these sites (Figure 13A). Correct insertion of the FLAG-hHP1α cDNA was confirmed by restriction digest of purified DNA clones (Figure 13B).

Creation of the transgenic flies with hHP1α-FLAG required microinjection of the pUASTattb hHP1A-FLAG plasmid into *Drosophila* embryos that harbour an attP site and express PhiC31 integrase, for PhiC31-mediated integration into the genome. In this system, plasmid containing an attB site is integrated into the genome at attP, by homologous recombination mediated via PhiC31 integrase. This process was trialled several times, by injecting freshly laid, dechorionated and dehydrated *Drosophila* embryos with the pUASTattB-hHP1α-FLAG plasmid using a microinjector. The eggs were then incubated overnight at 18°C with pressurised oxygen, before moving to 21°C for a further 24 hours. Surviving larvae were then gathered and grown in a standard vial to maturity at 25ºC. Unfortunately, although dozens of embryos were injected, none survived. The failure to obtain living larvae is likely due to excess dehydration of the embryos due to fluctuating temperatures in the laboratory, as faulty air-conditioning was unable to maintain the constant temperature that is critical for successful injections. Therefore, the prepared plasmid was sent to GenetiVision (Houston, TX) to commercially generate the transgenic fly line. Dr Helen Fitzsimons then carried out the required crossing with existing stocks to achieve the necessary genotypes, as described in Section 2.1.

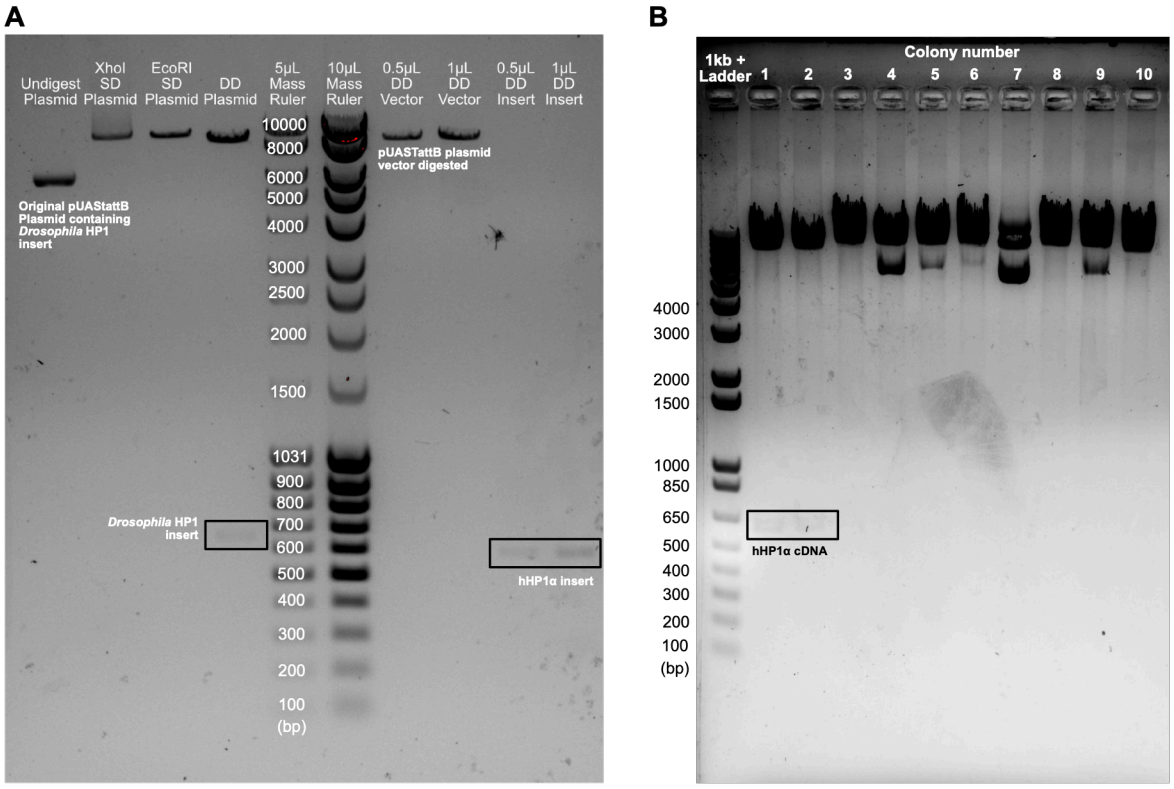

Figure 13: Cloning of human HP1α gene into pUASTattB plasmid.
A) 1% Agarose gel showing digestion of pUASTattB-DmHP1FLAG plasmid. Single digest (SD) of both XhoI and EcoRI cut once within the plasmid. Double digest (DD) of both EcoRI and XhoI cuts out the Flag-tagged dmHP1 insert at 660bp. Double digest of the gel-purified pUASTattB vector show removal of dmHP1-FLAG, and the PCR-amplified hHP1α insert show single band at 620bp B) Agarose gel showing double digest of DNA purified from DH5α colonies transformed with pUASTattb-hHP1FLAG plasmid. Colonies one and two show successful plasmid transformation.

The set of hHP1α expressing fly lines: hHP1α OE, hHP1α OE/dmHP1 KD, hHP1α OE/Csk KD and hHP1α OE/Csk KD/dmHP1 OE, were processed for immunohistochemistry using a FLAG antibody (Figure 14). The human HP1α transgene line in Figure 14A demonstrates cells with a strong FLAG signal co-localising with GFP fluorescence. The imaginal processing of discs for immunohistochemistry resulted in the distorted boundary line.

In flies with hHP1α and dmHP1 KD, the correct expression and localisation of human HP1α was observed, in conjunction with a strong, specific KD of endogenous dmHP1 along the A/P boundary (Figure 14B). The dmHP1 RNAi used to reduce the endogenous dmHP1 did not decrease the expression level of the hHP1α protein, unlike the reduced expression observed when over-expressing dmHP1 as the RNAi targets an mRNA sequence not found in hHP1α (Figure 14C). The hHP1α over-expression in conjunction with the malignant pathway activation resulting from Csk KD (Figure 14C) again showed correct A/P boundary localisation of hHP1α and constitutive expression of dmHP1 throughout the imaginal disc.

Unfortunately, there was contamination of the parental flies crossed to generate progeny larvae for immunofluorescence of the Csk KD/ dmHP1 KD/ hHP1α, and so the immunofluorescence data for this fly genotype will be collected as part of future work. As the larvae bred for the invasion assay were prepared separately from those used in the immunofluorescence experiments, this contamination had no bearing on the data collected for the invasion assay.

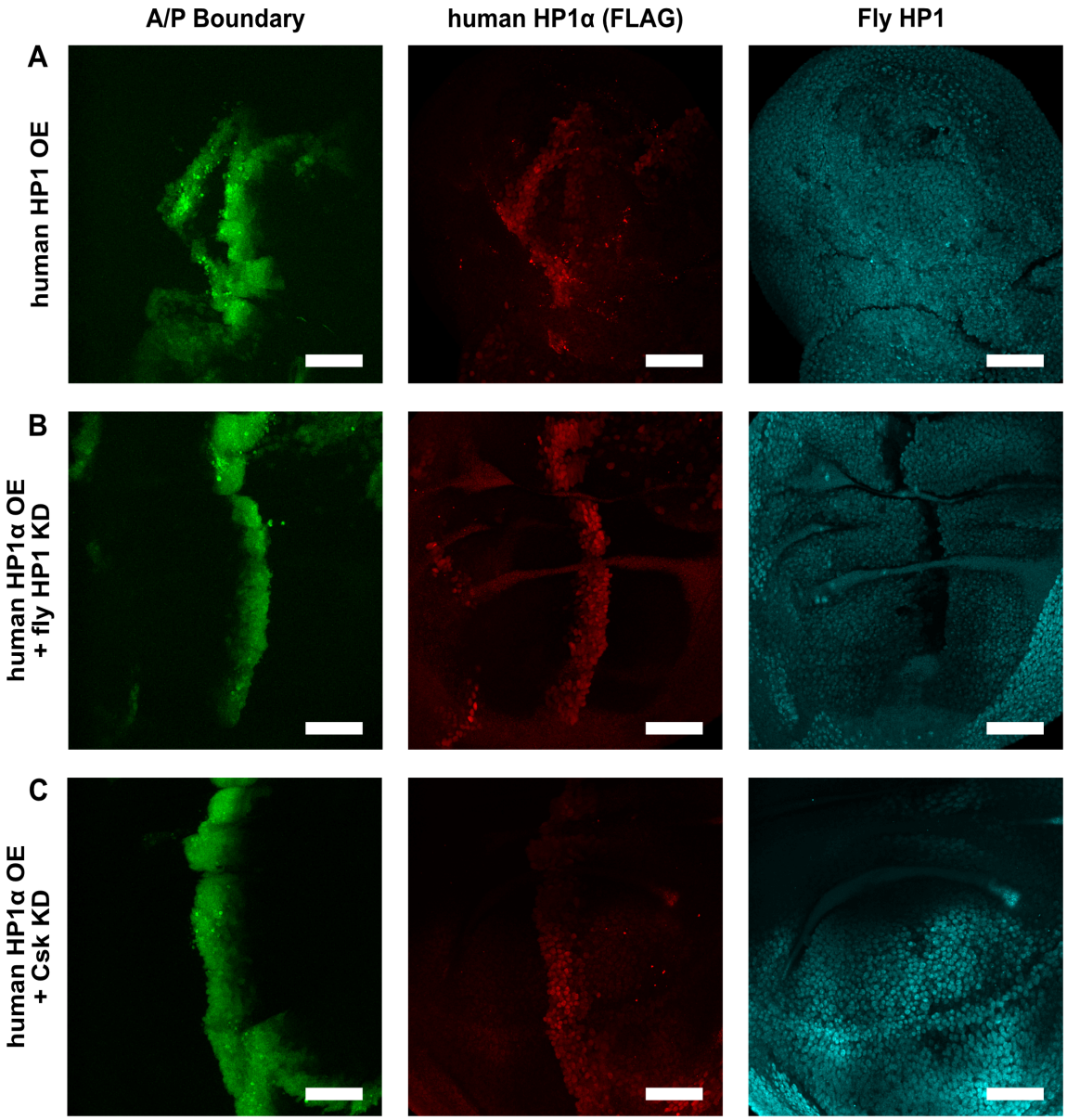

Figure 14: Immunohistochemistry of human HP1α transgenic fly larvae imaginal disc A/P boundaries

Maximum intensity z-stack projections of third instar *Drosophila* larvae that were processed for immunohistochemistry, using Rabbit anti-FLAG (Sigma F7425) primary antibody to detect FLAG-tagged dHP1. Alexa Fluor® 647-conjugated goat anti-rabbit IgG was used as the secondary antibody at 1/500 dilution. Confocal z-stack was collected over the height of the disc at 630x magnification. Scale bar = 50μm.

Figure 11 shows representative images of the invasive potential of the hHP1α expressing transgenic fly lines, and Figure 12 shows average invasive potential across biological replicates. In larvae without activation of the Src malignant pathway (no Csk KD), the levels of invasion resulting from expression of hHP1α either alone or in concert with dHP1 knockdown, appear to have increased in a manner similar to over expression of dmHP1 (17C and D), although there is a small increase in invasive potential. In Figure 11K, hHP1α over-expression results in an increase in invasion, over the Csk KD, and is more invasive than the phenotype resulting from over-expression of dmHP1 (Figure 11I). Expression of hHP1α in addition to KD of dmHP1 in a Csk KD background (Figure 11L) rescues the severely invasive phenotype of dmHP1 KD in a Csk KD background (Figure 11H). However, this phenotype displays more invasive characteristics than Csk KD alone (Figure 11G).

3.3: Discussion

Our previously established model of *Drosophila* cell invasion demonstrated the loss of dmHP1 had a synergistic effect with activation of the Src pathway to promote epithelial cell invasion. Importantly, overexpression of *Drosophila* HP1a and human HP1α could rescue the invasive phenotype resulting from knock down of CSK and dmHP1, demonstrating that it is a gene-specific effect. This confirms in the context of a tissue microenvironment that HP1α has a causal role in supressing cell invasion, in agreement with the work performed in breast cancer cells lines (D. A. Kirschmann et al., 2000).

Reflecting the correlation of HP1α loss in invasive thyroid tumours (Tretiakova et al., 2014), these findings indicate that a reduction in dmHP1 alone does not trigger cellular invasion, but when lost in conjunction with activation of a malignant pathway, it promotes invasive behaviour. However, the demonstration that overexpression of human HP1α can increase invasive potential in CSK KD cells suggests gene-dosage may also play a role in regulating HP1 function. It is possible that excessive hHP1α is dimerising with endogenous dmHP1 and preventing it from accessing the chromatin, importantly when dmHP1 is also lost expression of human HP1α does suppress invasion.

Since loss of HP1α is observed in invasive cells of many tumour types it will be of interest to test if HP1α is a general suppressor of malignant signalling pathways by activating other pathways known to promote tumorigenesis in our *Drosophila* epithelial cell model. In addition, this assay can now be used to explore the role of other genes identified as contributing to HP1α mediated suppression of metastasis.

Chapter 4: Impact of HP1α KD on the integrity of cancer cell nuclei

4.1: Introduction

MCF7 is a cell line dating back to the 1970's and derived from an invasive breast ductal carcinoma, which has a poorly invasive phenotype. Previous work in the laboratory established constitutive short hair-hairpin RNAi-mediated KD of HP1α and HP1ß in MCF7, as well as a scrambled shRNA control using Qiagen SureSilencing shRNA plasmids, and achieved a high level of KD efficiency as shown in Figure 15. These polyclonal cell culture populations were used to perform invasion assays through extra cellular matrix-like membranes, demonstrating that KD of HP1α resulted in a significant increase in invasive behaviour, as well as the lesser non-significant extent to which HP1ß did likewise.

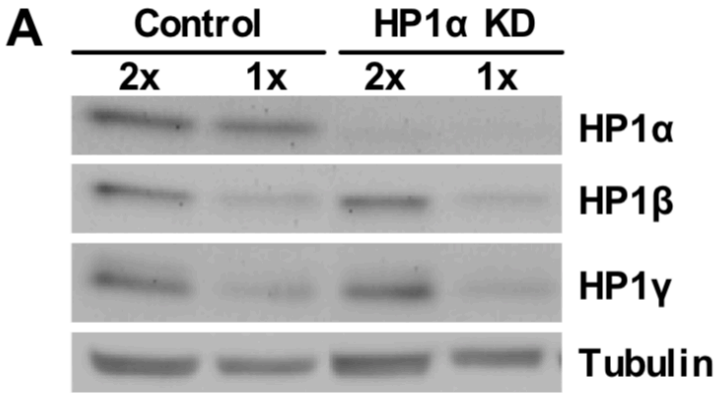

Figure 15: Protein level of HP1α in MCF7 cells with HP1 KD.

Reduced expression of the HP1 proteins was further explored using RNA-seq analysis to compare transcript levels of genes between KD and control MCF7 cells. HP1α KD resulted in 14.5% of 62,757 tested genes exhibiting differential expression. Genes were classified by Gene Ontology terms, which were used to identify the most prevalent groupings of differentially expressed genes; those involved with cell adhesion, migration and the actin cytoskeleton. By contrast, KD of HP1ß led to only 4.8% of genes being significantly ($p < 0.05$) differentially expressed, with the predominant GO term indicating genes involved with cell adhesion. Given the evidence indicating the greater cellular impact of HP1α loss, and increased invasion occurring in cells following it, this project will focus on the mechanics of HP1α in invasive cells, in favour of its less influential family member HP1ß.

4.2: Results

4.2.1: Changes in mechanical integrity of MCF7 cells with reduced HP1α

4.2.1.1: HP1α KD increases susceptibility to shear forces of MCF7 nuclei

To explore whether reduced HP1α KD alters the biophysical characteristics of the nuclear membrane the relative integrity of the nucleus of MCF7 control and HP1α KD cells following exposure to high mechanical shear forces by passaging a cell suspension through a fine gauge needle was tested. The experiment was performed using 1 mL of either MCF7 control of HP1α KD cells at a concentration of $1x10^2$ cells and passing the cell suspension through a 26G needle at constant rate of one cycle every 30 seconds, for a total of 70 passes. Aliquots of the cell suspensions were taken at intervals to count intact nuclei on a haemocytometer. Precedence in the literature has showed that the cell membrane of whole cells is fully disrupted and the nuclei released following the first two passages, and therefore subsequent counts and differences between the cell lines is due to differing nuclear characteristics alone, rather than a result of slower nuclei release from whole cells (Furusawa et al., 2015). This is consistent with results observed here, as no intact cells remain after 20 cycles. Figure 16 demonstrates that following exposure to shear forces, the MCF7 HP1α KD cells had fewer remaining whole nuclei after each cycle than control cells. The final count of intact nuclei following 70 passages through the needle resulted in HP1α KD cells having 35% the number of remaining nuclei in the MCF7 control. This suggests that HP1α KD makes the nuclear membrane more vulnerable to disruption by shear forces, reinforcing its role in the maintenance of peripheral heterochromatin, and provides evidence to pursue other methods such as atomic force microscopy to obtain quantifiable data. These results indicate that cells with HP1α KD have a nuclear periphery of altered integrity.

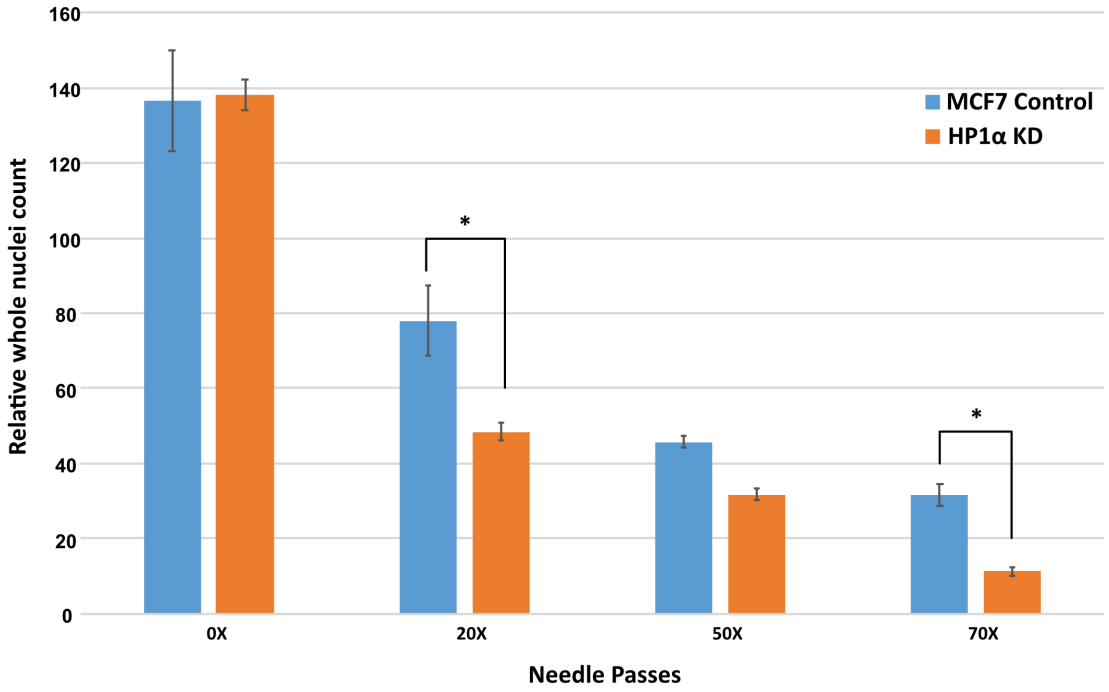

Figure 16: Graph of relative whole nuclei counts for MCF7 control or HP1α KD nuclei following passaging through a 26G needle.
Relative intact nuclei count for MCF7 control and HP1α KD cells following exposure to shear forces. Relative nuclei count calculated from mean numbers of intact nuclei from four fields of view at 100x magnification for each sample. * indicates p value <0.05.

4.2.1.2: KD of HP1α reduces the stiffness of the nuclear membrane

To further investigate the biophysical properties such as cellular elasticity and stiffness, resulting from loss of HP1α, atomic force microscopy (AFM) was used to physically probe cells for physical characteristics. Initially in collaboration with A/P Mark Waterland and Sam Brooke (School of Fundamental Sciences, Massey University), a Nanosurf FlexAFM system was tested for use in gathering mechanical property data of MCF7 whole cells settled on poly-D-lysine coated microscope slides, in a PBS solution. Following optimisation of the AFM to enable liquid immersion scanning, as well as several tests of dry scanning, liquid immersion and optimising the substrate for growing cells, the equipment did not meet the requirements for the experiment. The primary issue stemmed from the Z-depth rating of the Nanosurf FlexAFM, which allows for 5µm deflection of the cantilever above the surface of the imaged material, this was a major drawback as the Z-depth of an average MCF7 cell, depending on how it affixed the surface, can be upwards of 20µm. A topological scan could not be completed, positioning of the sampling grid correctly was impractical and unreliable with the particular equipment.

Therefore, a collaboration with Prof Bill Williams, Susav Pradhan (School of Fundamental Sciences and Dr Gleb Yakubov of the (University of Queensland) was undertaken to perform the measurements at the University of Queensland a JPK NanoWizard 3 Bioscience AFM. This AFM is specialised for cell-scale work, with integrated inverted microscope optics and fluorescent capabilities for fine positioning of the cantilever, and large Z-axis range. The MCF7 control and HP1α KD cells were transported to Dr Yakubov's laboratory. To ensure that the biophysical properties detected were those of the nuclei themselves, without the cell membrane and cytoplasmic components adding additional layers of confounding data, AFM data was collected on isolated nuclei (Figure 18).

A full force mapping procedure was performed on a single nucleus from MCF7 control or HP1α KD cells, where the pressure measurements with a cantilever force of 0.3nN was applied at each point in a 34x34 grid across the entire surface of the nucleus (Figure 17). This data shows a topological surface map of the nuclei, as well as regional variation in biophysical properties. The slope map of the MCF7 control nucleus, which indicates relative surface stiffness, shows a greater degree of heterogeneity when compared to the HP1α KD nucleus, as well as increased average stiffness. The patterning of the slope map for the MCF7 control nucleus also indicates underlying regions of denser material within the nucleus, compared to the more uniform and flexible HP1α KD control sample. Figure 17 also shows that the HP1α KD nucleus has a greater degree of tip adhesion across the surface, compared to the control nucleus, although it is more uniform in its pattern. This could indicate changes in expressed surface proteins following HP1α KD, that alter the probe adhesion. Scanning electron microscopy of the surface of these nuclei confirm a loss in exterior membrane complexity, and a decrease in surface pore complexes (Figure 18) while also appearing less structurally cohesive, with greater amounts of loose membrane material that can account for increased tip adhesion during atomic force microscopy.

To determine the elastic characteristics of the membrane, 17 individual nuclei from MCF7 control and HP1α KD cells were probed at three different points across their surface, and at each point tested with 0.3nN, 0.5nN and 1nN of applied force from the cantilever. These applied forces range over the lower and upper limits of force able to be applied by optical tweezers in a parallel experiment, to enable comparison of measurements between the two techniques. Figure 19 quantifies the distinct difference in both average stiffness and variation

between individual MCF7 control or HP1α KD nuclei. MCF7 control nuclei have a consistently higher Youngs modulus, a measure of elasticity, of around 15-25kPa over the range of applied forces, compared to 1-2kPa for HP1α KD nuclei. Moreover, HP1α KD nuclei are significantly more homogenous, with all samples displaying a similar level of low stiffness and increased elasticity. This data demonstrates s a ~20kPa decrease of the Youngs modulus, increasing the elasticity of the nuclear membrane of HP1α KD cells.

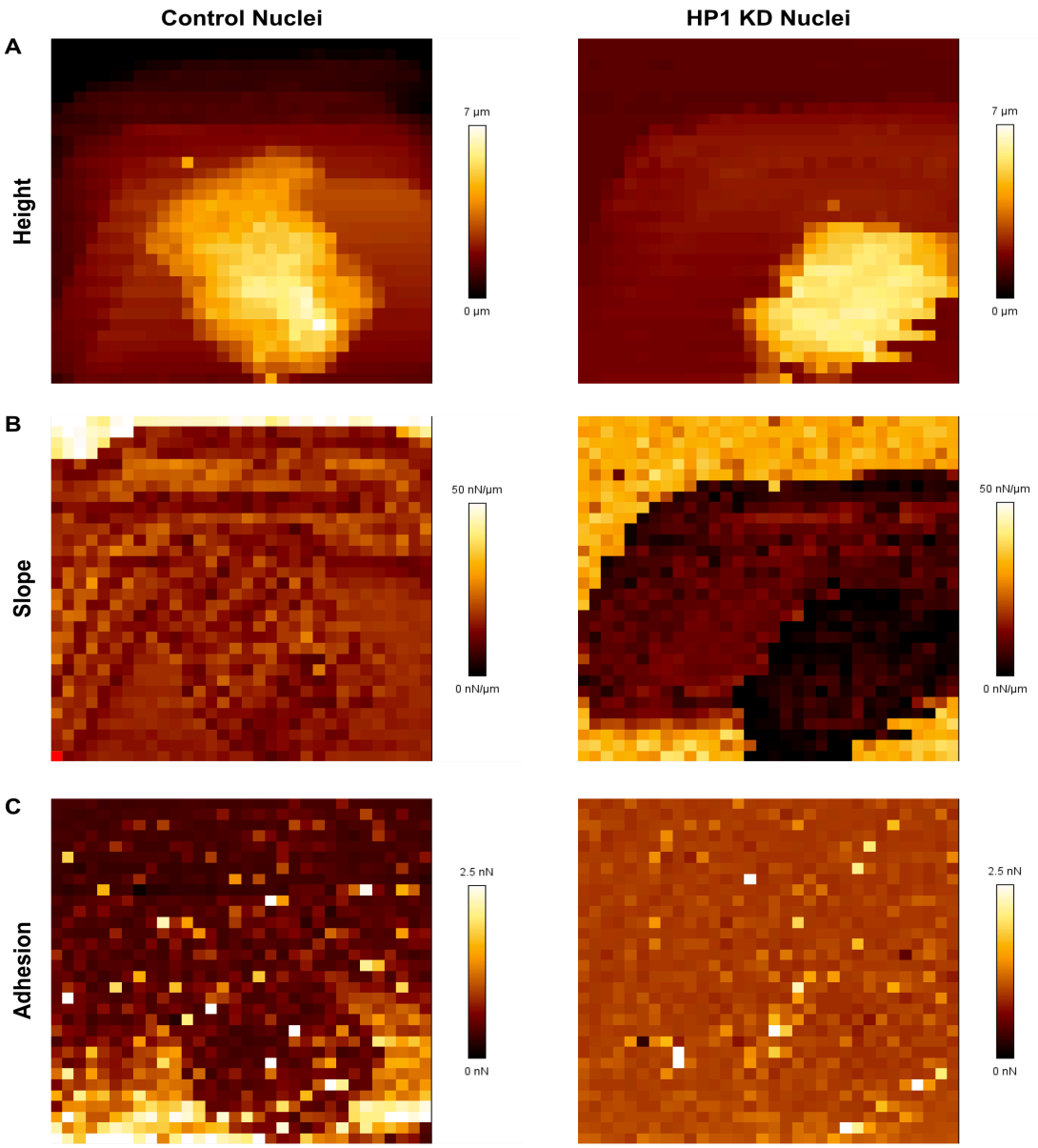

Figure 17: AFM Force Mapping of MCF7 control and HP1α KD nuclei
A) AFM map scan measuring height of first contact with the AFM tip, to map the surface topology of the nuclei. B) Map of slope readings, indicating resistance to the tip, stiffer areas are displayed as white, easily deformed areas as black. C) Adhesion map of nuclei, indicating degree of retention of the tip to the surface of the nuclei, 'stickier' areas displayed as white, reduced adhesion displayed as black. All data was collected from nuclei settled in a glass dish, submerged in a wash buffer.

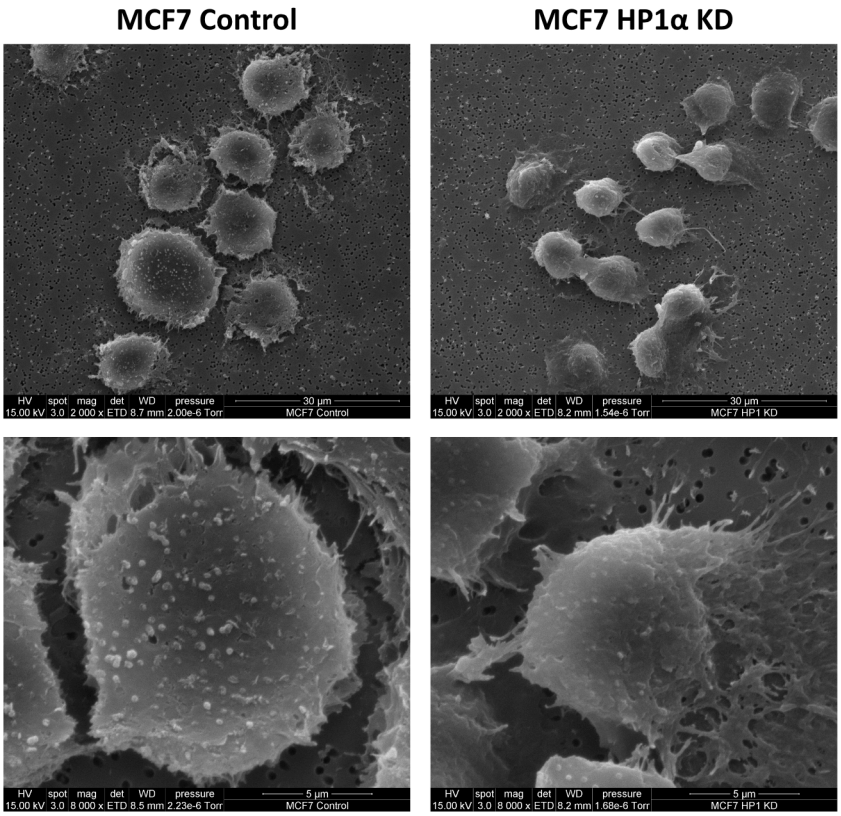

Figure 18: Scanning electron microscopy of isolated MCF7 control and HP1α KD nuclei
MCF7 control and HP1α KD nuclei on 0.4μm pore membrane filter, imaged on a scanning electron microscope with 15kV accelerating voltage.

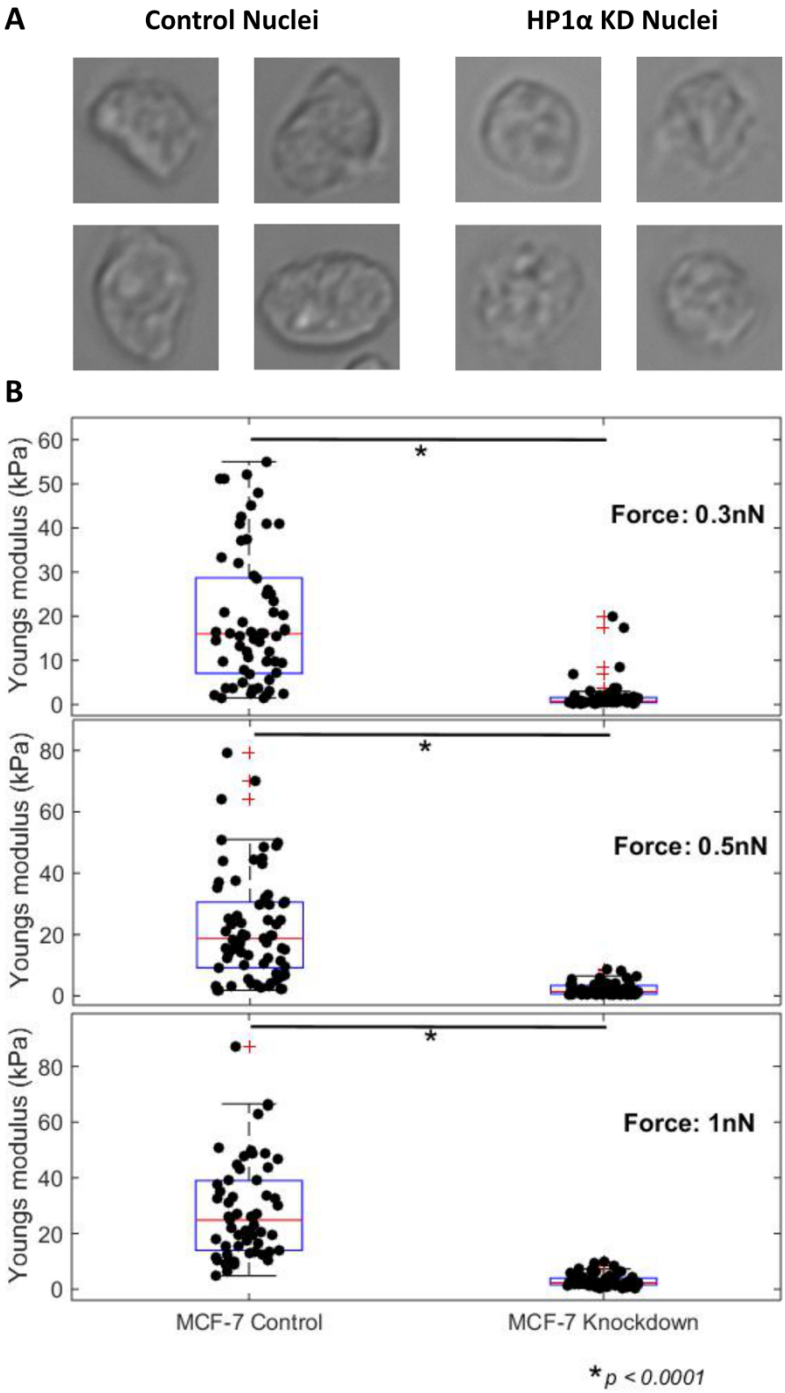

Figure 19: Youngs elastic modulus of MCF7 control and HP1α KD nuclei
A) Representative bright-field microscopy images of the isolated nuclei selected for AFM analysis. Field of view is 25x25μm. B) Calculated Youngs elastic modulus from AFM slope data (performed by Susav Pradhan) from 17 individual isolated nuclei from both MCF7 Control and HP1α KD cells, measured at an approach force of 0.3nN, 0.5nN or 1nN.

4.2.2: Characterisation of the nuclear periphery upon reduction of HP1α expression

4.2.2.1: Disrupted lamina in MCF7 HP1α KD cells

Due to the observed changes in the mechanical integrity of the nuclei of MCF7 HP1 KD cells, alterations to the nuclear lamina were examined. Changes in Lamin A/C and lamin B1/2 expression and localisation were examined using immunofluorescent confocal microscopy.

As shown in Figure 20 lamin A and C reveal consistent morphological differences between asynchronously growing MCF77 control and HP1α KΔ cells. These images reveal consistent morphological differences between asynchronously growing MCF7 control and HP1α KD cells. Maximum projections of the confocal Z-stacks show the MCF7 control cells exhibit a smooth lamin A/C layer (Figure 20A), with sporadic foci of lamin A/C invaginations within the nucleus identified in single layer slices (Figure 20B). By contrast, MCF7 HP1α KD cells have a highly crinkled and rumpled lamin A/C layer (Figure 20A) with an increase in punctate foci visible in the cross section (Figure 20B).

Immunofluorescence of lamin B2 (Figure 21) showed the MCF7 control cells displayed a smooth lamin B2 layer (Figure 21A), while HP1α KD cells had slightly increased crinkling visible at the peripheries of the nucleus. However, HP1α KD cells did display more frequent occurrences of lamin B2 invaginations and creasing (when compared to the MCF7 control cells), particularly visible when observing the cross section of the nuclei (Figure 21B).

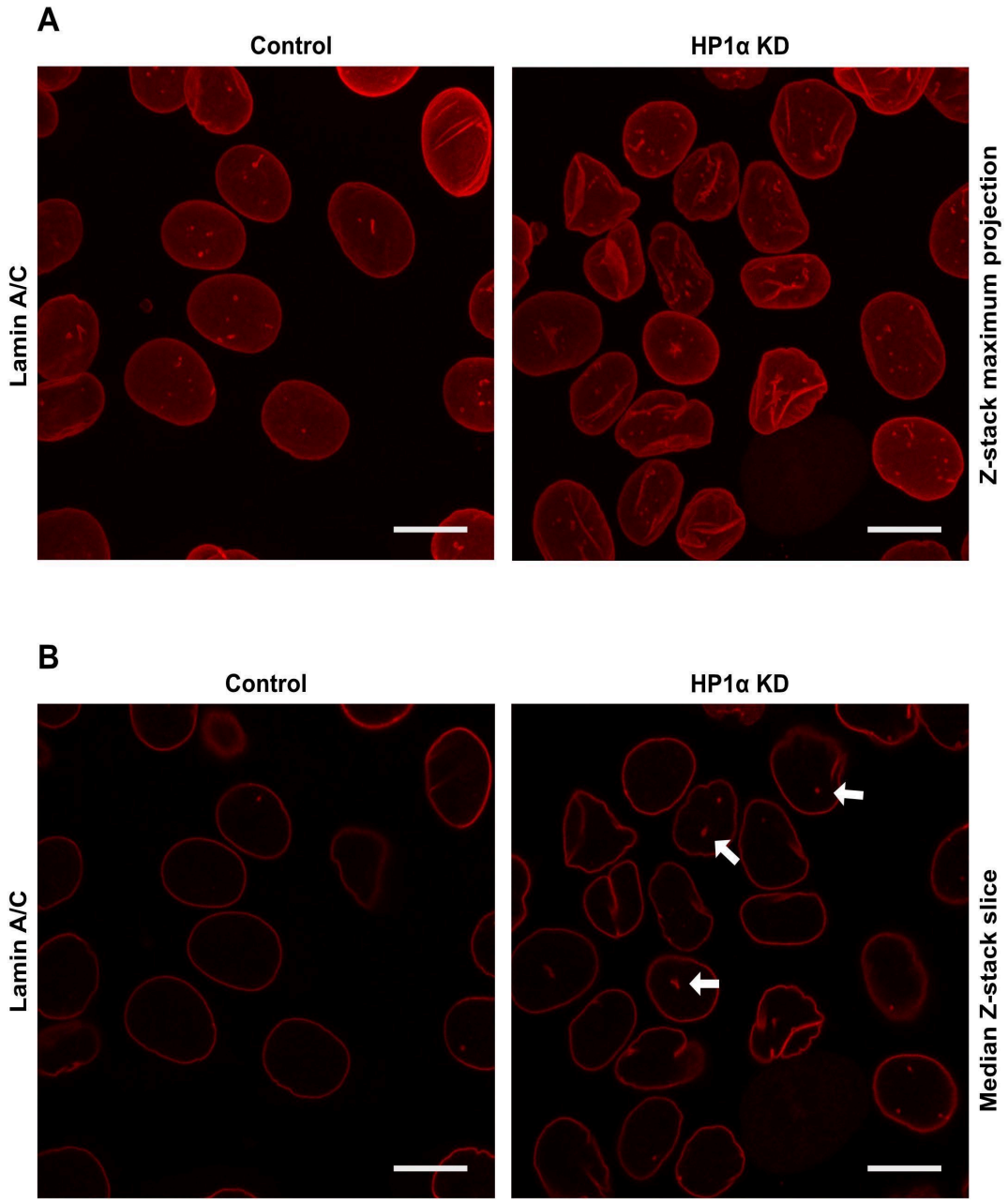

Figure 20: KD of HP1α results in crumpling and distortion of Lamin A/C meshwork
MCF7 control or HP1α KD were processed for immunofluorescence microscopy using a primary antibody against lamin A/C. Alexa Fluor® 647-conjugated goat anti-rabbit IgG was used as the secondary antibody. Scale bar: 10μm. **A)** Maximum intensity projection of confocal z-stack. **B)** Medial confocal slice of nuclei projection. Representative images of two biological replicates. Arrows indicate lamin A/C invaginations.

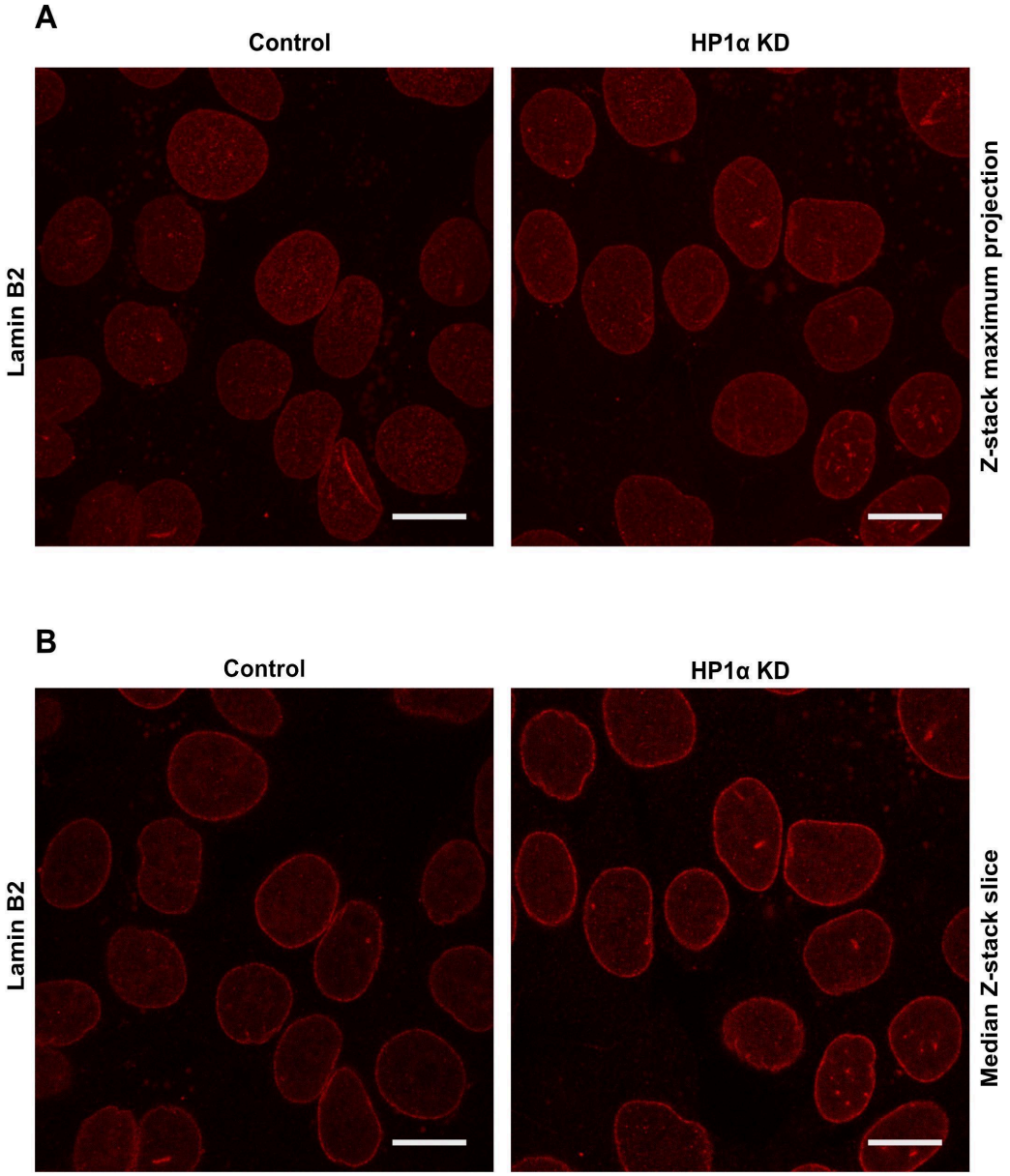

Figure 21: KD of HP1α results in increased punctuate foci of lamin B2 protein within the nucleus.
MCF7 control or HP1α KD cells were processed for immunofluorescence microscopy using a primary antibody against lamin B2. Alexa Fluor® 647-conjugated goat anti-rabbit IgG was used as the secondary antibody. Scale bar: 10μm. A) Maximum intensity projection of confocal z-stack. B) Medial confocal slice of nuclei projection. Representative images of two biological replicates.

Unfortunately, the lamin B1 antibody used in this study has proved unsatisfactory for immunofluorescence staining, with neither fixation in 4% paraformaldehyde nor methanol providing sufficient epitope specificity. Both fixation methods were tested as fixation is known to have different effects on epitope recognition (Figure 22A and 22B).

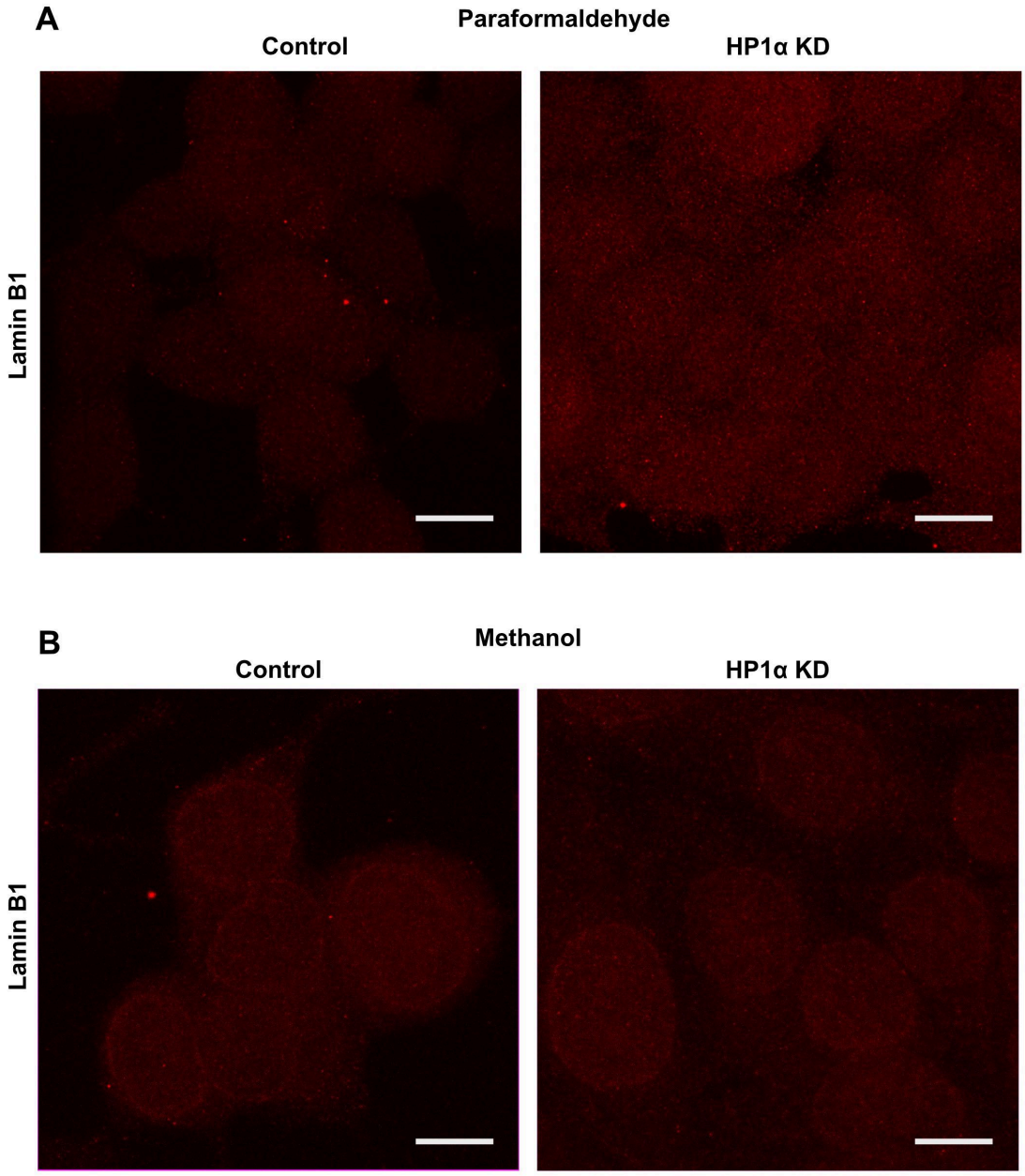

Figure 22: Different fixation methods did not improve lamin B 1 antibody epitope specificity
MCF7 control or HP1α KD cells were processed for immunofluorescence microscopy using a primary antibody against lamin B1. A) Fixation of cells in 4% PFA B) Fixation of cells in -20ºC methanol. Alexa Fluor® 647-conjugated goat anti-rabbit IgG was used as the secondary antibody. Maximum intensity z-stack projections, with scale bar: at 10μm.

4.2.2.2: Increasing solubility of lamins upon HP1α KD

To investigate if the altered lamina morphology observed in Figure 21 and 26 is due to disruption of lamin localisation, MCF7 control and HP1α KD cells were fractionated into whole, cytoplasmic and nuclear fractions. In addition, a nuclear envelope fraction was also isolated using a commercial isolation kit (Section 2.11). To ensure the fractionation of cellular

components was successful, a western blot was performed with antibodies directed against the cytoskeletal protein tubulin and the nuclear-localised histone H3. Figure 23A shows the presence of tubulin in the whole cell lysate and cytoplasmic fraction as expected. Figure 23B shows histone H3 present in the nuclear fraction. While lamin B2 is usually used as a loading the control for nuclear envelope extracts, its localisation may be disrupted in response to HP1α KD, so loading of equal total protein for the nuclear isolates was demonstrated using Coomassie staining, after separation on a 10% SDS PAGE (Figure 23C). This gel showed equivalent amounts of total protein present in each sample, although there were some distinct changes in some protein band intensities.

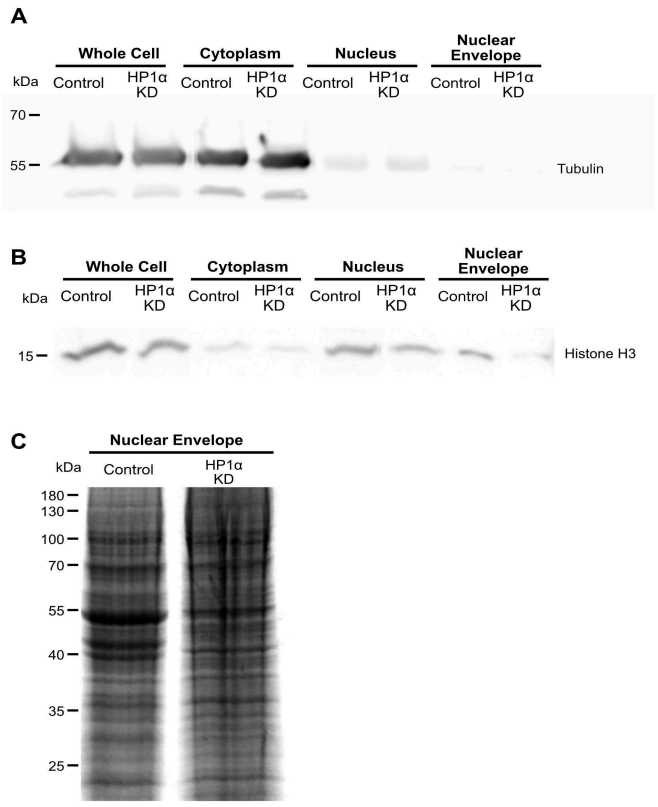

Figure 23: Western blot fractionation and loading controls for MCF7 cell fractions and nuclear envelope protein isolation
A) Western blot of cell lysate fractionation and nuclear envelope protein probed for α-Tubulin. 50kDa Tubulin is observed only in whole cell and cytoplasmic fractions, in equal amounts for control and HP1α KD. B) Western blot probing for Histone H3, shows a successful fractionation of nuclear core histones from the cytoplasmic lysate. C) Coomassie staining of 10% SDS PAGE separating 25μl of nuclear envelope samples of MCF7 control and HP1α KD cells.

Figure 24A shows that there is a marked reduction in the level of lamin A/C in the nuclear envelope in the MCF7 HP1α KD cells. Despite this, similar levels of lamin A/C are observed in the whole cell lysates, as well as in the nuclear fractions of both cell lines. Therefore, it does not appear that the total nuclear level of A/C-type lamins has been altered in the nucleus when

HP1α has been knocked down.

These MCF7 control and HP1α KD cell fractions were also probed for lamin B2. Figure 24B shows similar levels between the control and HP1α KD of lamin B2 levels in the whole cell and nuclear fraction, at the expected molecular weight of 72kDa. Similar to the pattern observed with lamin A/C (Figure 24A) there is a substantial decrease in the amount of lamin B2 in the nuclear envelope fraction of HP1α KD cells compared to the MCF7 controls.

The notable reduction of lamin A/C and B2 in the nuclear envelope of the HP1α KD suggests this network of lamins is more loosely attached to the nuclear membrane.

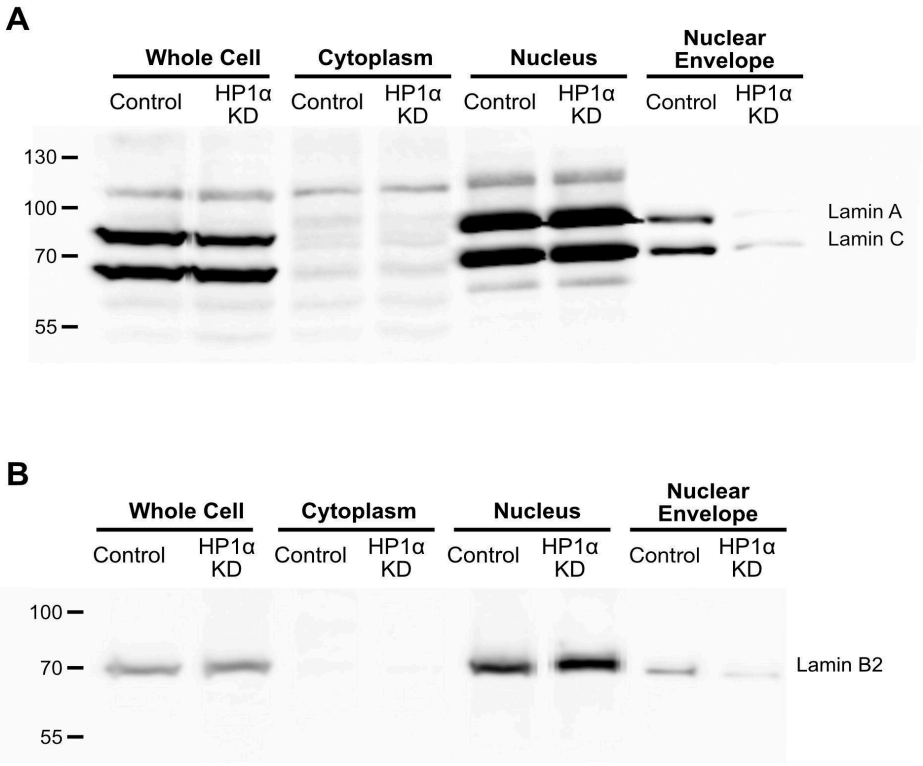

Figure 24: MCF7 cells have reduced retention of lamina proteins A/C and B2 to the isolated nuclear membrane following KD of HP1α
A) Western blot of cell lysate fractionation and isolated nuclear envelope protein probed for lamin A/C, demonstrating equal levels of lamin A/C in whole cells, and successful fractionation of nuclear components, yet significantly decreased levels of lamin A (~74kDa) and lamin C (~63kDa) in the HP1α KD cells. B) Western blot as for A, probing for lamin B2 showing a decrease in lamin B2 (~68kDa) isolated with the nuclear membrane material in HP1α KD cells.

To this end, a salt solubility assay (Section 2.15) was used to detect how soluble the lamin proteins were. Isolated nuclei of asynchronously grown MCF7 control and HP1α KD cells

were incubated with increasing salt concentrations (from 50-500mM NaCl). Aliquots of the supernatant for each salt concentration were separated by 10% SDS PAGE and probed via western blot for lamin A/C or lamin B2. The 150mM NaCl fraction from HP1α KD shows lamin C and a higher proportion of lamin A present compared to the control (Figure 25A). While lamin B2 is detected in the lower salt fractions in HP1α KD nuclei, it is present in the 250mM NaCl and above in the control nuclei (Figure 25B). This result indicates that the KD of HP1α is associated with increased solubility of lamin A/C and B2 in increased salt concentrations.

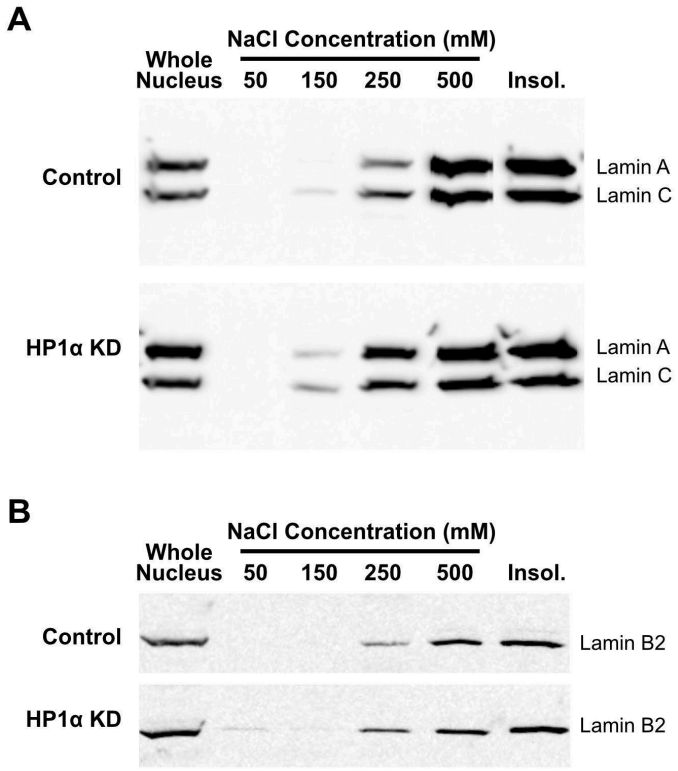

Figure 25: Lamin protein solubility increases in whole nuclei with HP1α in response to titrated salt concentrations.
Western blot of salt supernatants following incubation of isolated whole nuclei, to detect relative degrees of detachment of the nuclear lamina between MCF7 control cells and those with HP1α KD. A) Western blot probed for lamin A/C. B) Western blot probed for lamin B2.

4.2.2.3: Visualising the nuclear lamina

To further probe the differences in chromatin and nuclear envelope architecture in MCF7 control and HP1α KD cells, transmission electron microscopy was used. These cells were mixed in 3% agar and centrifuged to form a pellet, which was then processed for transmission electron microscopy (Section 2.16). Figure 26 compares the chromatin formation at the

nuclear membrane periphery, with darker regions indicating denser regions of chromatin. The MCF7 control cells exhibit distinctly denser chromatin clusters at, and extending away from, the nuclear periphery. By contrast, HP1α KD cells lack distinct heterochromatin regions abutting the membrane, with a more homogenous staining pattern.

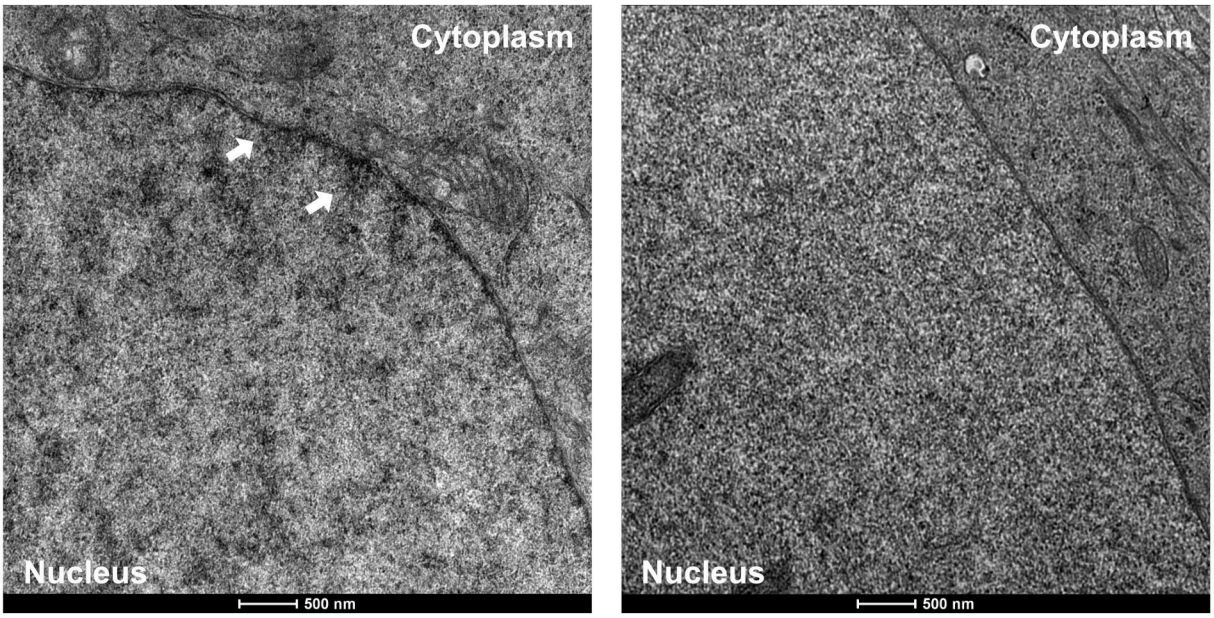

Figure 26: Transmission electron microscopy of the nuclear membrane
A) Representative transmission electron microscopy image of MCF7 control and HP1α KD cells. Arrows indicate dense regions of heterochromatin. 34000x magnification.

To visualise the disruption of the lamina at higher resolution a procedure for immuno-labelled transmission electron microscopy was developed. Several approaches were taken to prepare the material for imaging. Asynchronously growing MCF7 control and HP1α KD cells were harvested and embedded in an agar pellet. This pellet was then sectioned into 15-20µm slices using a cryotome, with the assistance of Dr Matthew Perrot and Saritha Gils (Massey University, School of Veterinary Science). These sections were then stained with the antibody raised against lamin B2 before staining with an IgG secondary antibody with conjugated 10 nm gold beads. These slices were then embedded in resin and sectioned to 90nm on the ultramicrotome. Alternately the cells were grown directly on glass slides, which were then stained and embedded directly on the surface.

The gold beads provide extremely dense consistently sized 10nm dots to identify protein localisation when viewed with a transmission electron microscope. As the beads are so small in comparison to the scale of a mammalian cell (Figure 27A), multiple high magnification

images scanning across the area of the cell are required to map the bead locations (Figure 27A and B). These separate images and plotted bead locations can then be digitally stitched together and overlayed on a lower magnification image (Figure 27C).

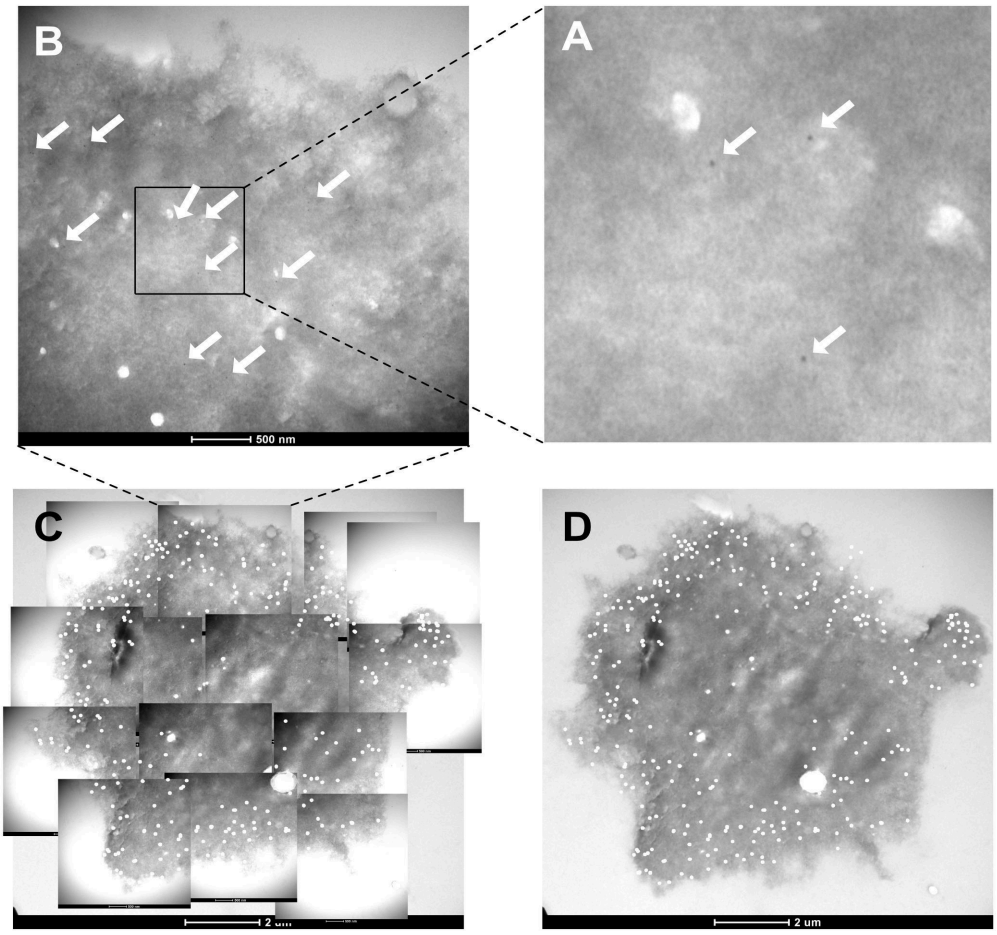

Figure 27: Process to analyse immune-EM sample
A-B) Digitally magnified image of MCF7 control cell stained with lamin B2 antibody, with 10nm gold colloidal bead-conjugated secondary antibody. 43000x magnification C) High magnification images overlayed on a 11500x magnification image with 10nm beads highlighted. D) Overview of the whole cell with protein target locations visible

Unfortunately, time and resources did not allow the full collection of comparable samples, owing to further cell permeation optimisation required for the secondary gold-conjugated antibody. This technique would also be improved by serial sectioning of the embedded cells to prevent inappropriate comparison between samples taken at very different heights of the cell monolayer, where the tip of the nuclei may be all that is visible, depending on the section. Serial sectioning would provide a sequencing of slices moving from the outside to towards the centre of the cell layer.

4.2.2.4: HP1α KD Alters the Association of Proteins to the Nuclear Membrane

While the nuclear lamina is adjacent to the nuclear membrane, many proteins are integrated into the membrane itself and also interact with the lamina meshwork.

The lamin B receptor (LBR), is integrated into the nuclear membrane and interacts with both the lamin B proteins and chromatin proteins, including HP1α. Localisation of LBR was determined by cellular fractionation of MCF7 control and KD cells, and immunoblotting with an LBR antibody. During the fractionation process the whole nuclei were exposed to a high salt concentration to collect soluble protein, before final lysis (Figure 28A). Similarly, to the lamin A/C and B2 proteins (Figure 24), LBR showed a marked loss in retention by the nuclear membrane through the isolation process, as well as indicating increased solubility following HP1α KD (Figure 28A). When MCF7 control and HP1α KD cells were stained for LBR and observed as a maximum projection confocal z-stack, there is a reduction in cytoplasm associated LBR following HP1α KD (Figure 28B).

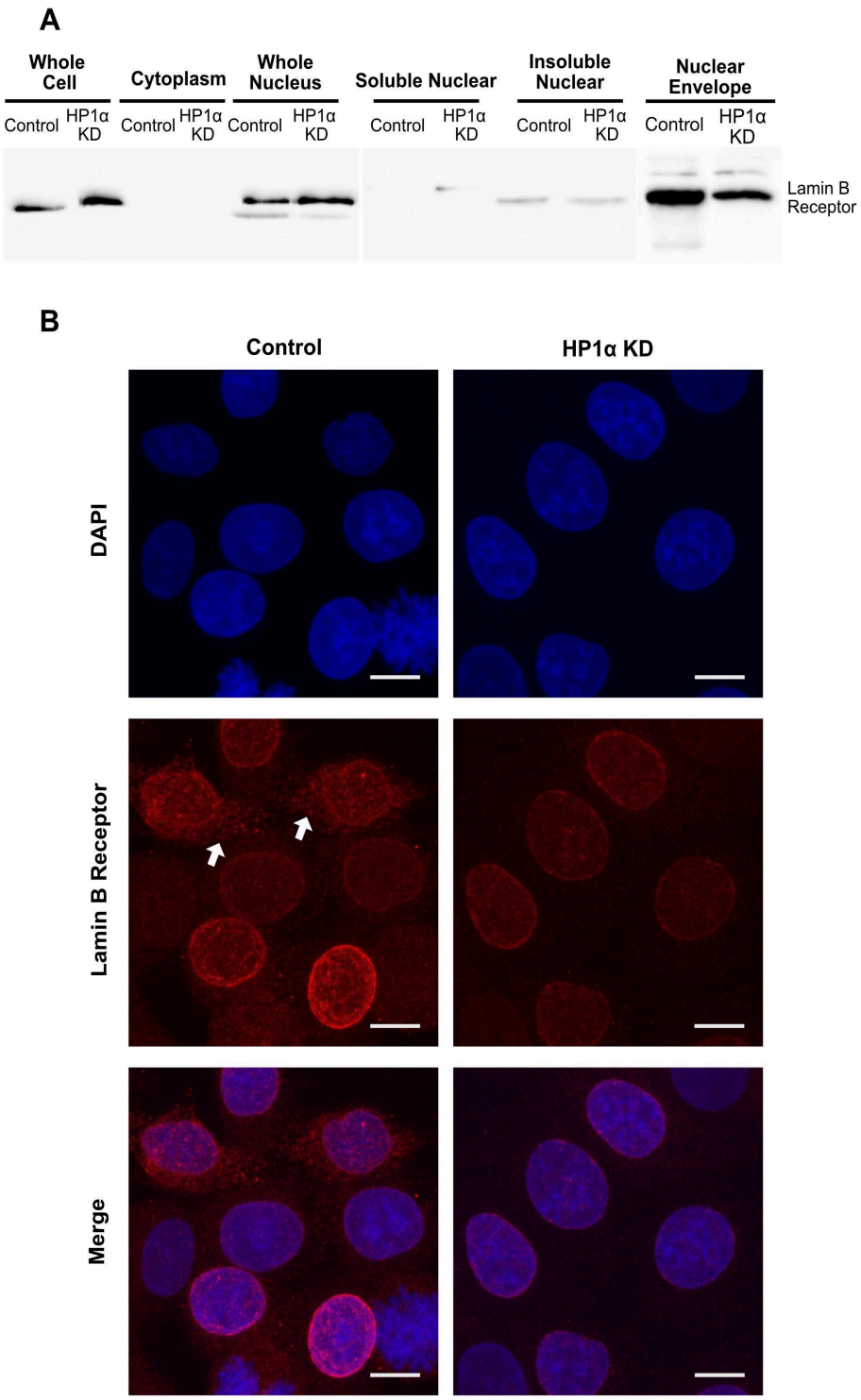

Figure 28: Lamin B receptor protein has decreased nuclear membrane retention and endoplasmic reticulum presence in MCF7 cells following HP1α KD

A) Western blot of MCF7 control or HP1α KD cell fractionation and isolated nuclear envelope protein probed for lamin B receptor demonstrating reduced retention of lamin B receptor to the nuclear membrane. B) MCF7 control or HP1α KD cells were prepared for immunofluorescence microscopy using a primary antibody against the lamin B receptor protein. Alexa Fluor® 647-conjugated goat anti-rabbit IgG was used as the secondary antibody at Scale bar: 10μm. Maximum intensity z-stack projection. Lamin B receptor shows reduced endoplasmic reticulum presence following reduction of HP1α (arrows indicate endoplasmic reticulum localisation).

To identify changes in proteins in the nuclear membrane in MCF7 control and HP1α KD cells,

and in particular, the nuclear envelope lysates that showed a decrease in retention of many membrane-associated proteins (Figure 24 and 28). Coomassie staining of these nuclear membrane samples showed distinct changes in intensity of several bands between the MCF7 control and HP1α KD cells, and so a selection of these bands was excised and prepared for protein identification via mass spectroscopy as described in section 2.17 (Figure 29).

This data will inform future research on the major differences in protein retention during membrane isolation and provide specific candidate proteins for an investigation into modulators of nuclear membrane stability.

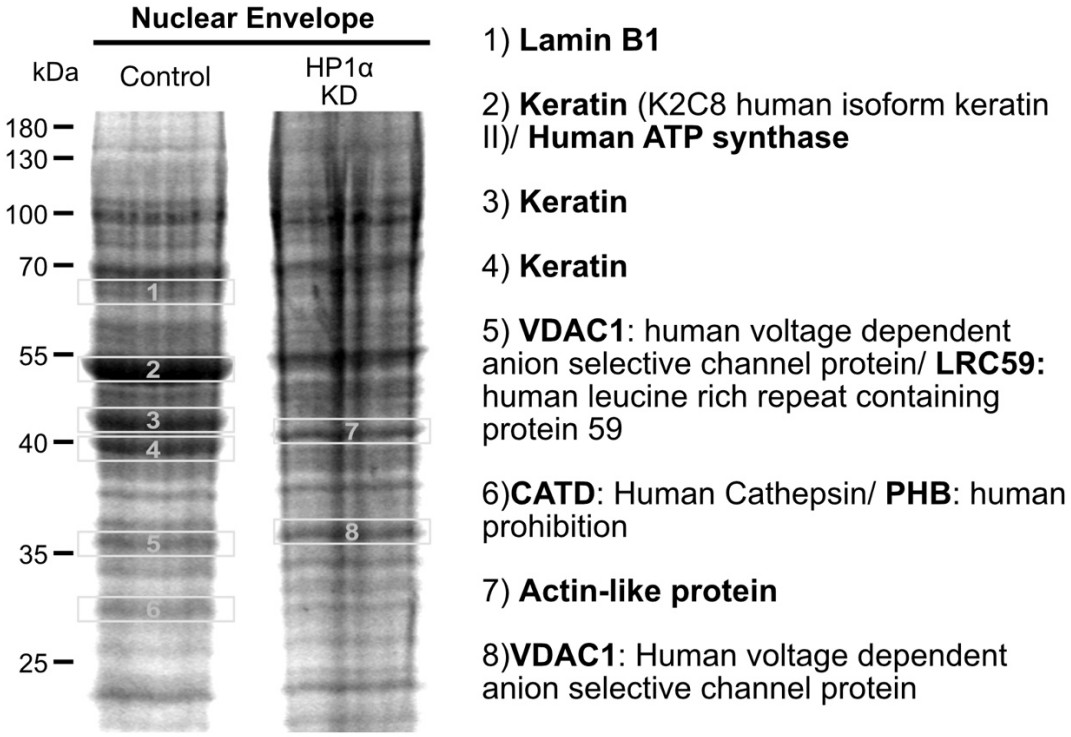

Figure 29: Nuclear envelope proteins for identification by mass spectroscopy
Coomassie staining of 10% acrylamide gel separating 25μl of nuclear envelope samples of MCF7 control and HP1α KD cells. Labelled with bands that were excised for mass spectroscopy analysis.

In a candidate approach, other membrane associated proteins that interact with the lamina were visualised with immunofluorescence to observe changes in localisation following HP1α KD in MCF7 cells.

Emerin is an integral membrane protein that associates with A-type lamins and facilitates their interaction with the membrane (Sullivan et al., 1999). Comparison of the MCF7 control and HP1α KD cells immuno-stained for emerin in Figure 30A show a similar localisation, however KD of HP1α increases the number of cytoplasmic foci resulting from blebbing of the nuclear

membrane, indicating loss of localisation following reduction of HP1α.

Additional proteins of interest included BAF (barrier-to-autointegration factor) which interacts with many nuclear membrane-associated proteins including emerin (Vlcek et al., 2001), and bind directly to DNA, linking chromatin to the nuclear periphery (Figure 30B). By contrast the HGMN5 (Figure 30C) protein is associated with chromatin decompaction and has been associated with loss of nuclear membrane sturdiness (Furusawa et al., 2015), making it a key candidate for involvement in destabilising the nuclear membrane. Another protein that interacts with both the lamina and HP1α is PRR14, making it a key candidate intermediary transmitting change in HP1α expression to the lamina that results in changes of biophysical properties (Figure 30D). Unfortunately, these antibodies lacked epitope specificity for reliable comparison using immunocytochemistry and require further optimisation.

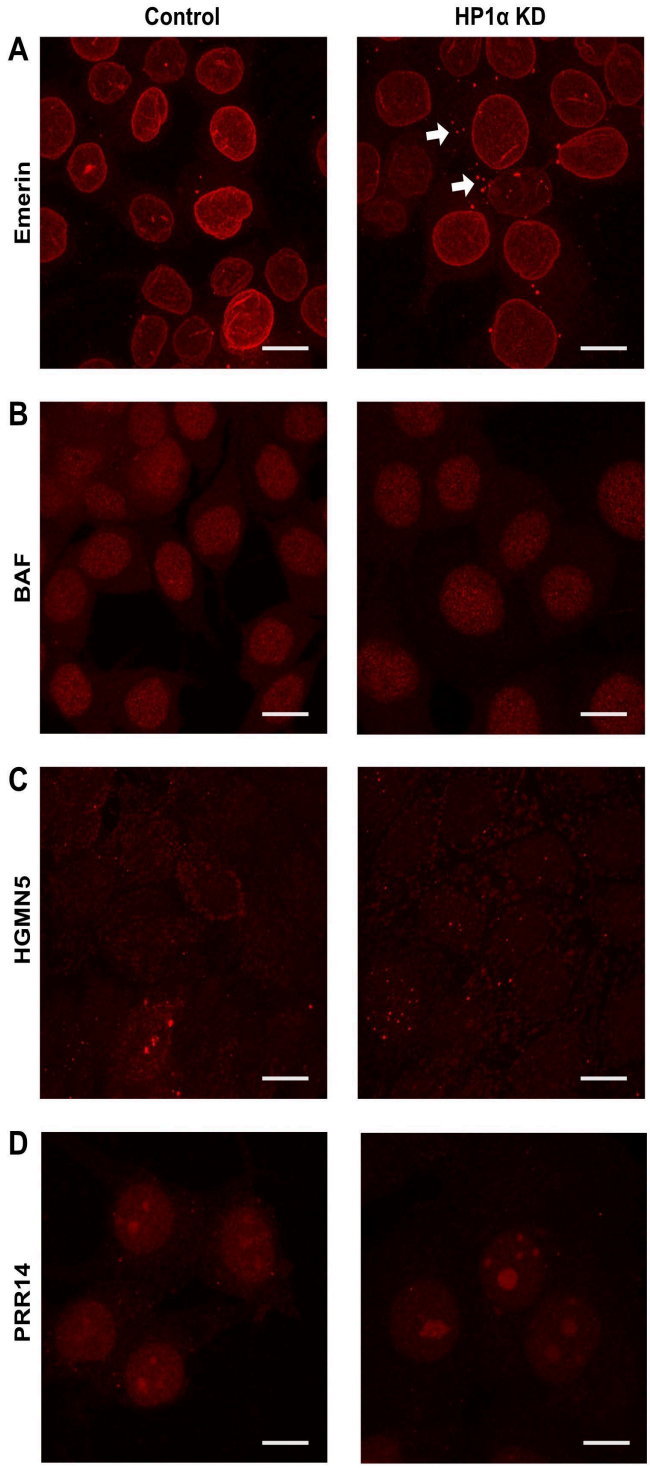

Figure 30: Immunofluorescence confocal microscopy of nuclear membrane-associated candidate proteins

MCF7 control or HP1α KD were processed for immunofluorescence microscopy and probed for candidate nuclear membrane-associated proteins. Alexa Fluor 647-conjugated goat anti-rabbit IgG was used as the secondary antibody at 1/500. Scale bar: 10μm. A) Maximum projection Z stack of cells stained for integral nuclear membrane protein emerin. Loss of HP1α is associated with an increase in extra-nuclear emerin foci. B) Cross section slice of MCF7 control and HP1α KD cells probed for barrier-to-autointegration factor (BAF), showing similar localisation and morphology between samples. C) Cross section slice of MCF7 control and HP1α KD stained for HGMN5, with poor epitope specificity. D) Cross section slice of MCF7 control and HP1α KD cells stained for PRR14.

4.3: Discussion

Invasive breast cancer cells must deform their nuclei to squeeze through interstitial spaces, this reduction nuclear envelope integrity is a characteristic that enables cell migration (Olins et al., 2008). Since loss of HP1α expression has been associated with invasive tumour cells, this chapter explored how the reduction of HP1α may destabilise the nuclear membrane via loss of heterochromatin integrity to assist invasion. Reducing HP1α expression in poorly invasive MCF7 breast cancer cells significantly increased their nuclear membrane flexibility and decreased the interior nuclear complexity and heterogeneity by atomic force microscopy. This decrease the complexity of nuclear interior is associated with changes in heterochromatin patterning that includes a decrease in peripheral heterochromatin. Unlike the Furusawa et al. (2015) study, loss of heterochromatin also influences the morphology of the nuclear lamina.

While the expression of the proteins that make up the lamina, Lamin A, C and B2, is unchanged with HP1α KD they have increased solubility from the meshwork and weakened interactions with the nuclear membrane, as shown by immunoblot comparing co-extraction of membrane associated proteins in isolated membrane fragments (Dahl, Kahn, Wilson, & Discher, 2004). Lamins A/C in particular display significant disorganisation following KD of HP1α by immunofluorescent staining. Other membrane proteins that act as intermediaries between HP1α, chromatin, and the lamina display changes in localisation if not expression levels, such as LBR and emerin, which both act to target and maintain the lamina meshwork and peripheral heterochromatin interactions.

These findings demonstrate how HP1α can suppress cell migration through maintaining the integrity of peripheral heterochromatin and thus the stability of the nucleoskeleton.

Chapter 5: Discussion

In agreement with immunohistochemical screening of tumour arrays, reduction of HP1a expression is associated with an increase invasion. Modulating of the level of the heterochromatin enriched HP1α protein in cancer cell lines (D. A. Kirschmann et al., 2000) and a *Drosophila* model of cell invasion, has clearly demonstrated that HP1α suppresses malignant cell invasion, presumably in part by creating a more permissive chromatin environment and dysregulating gene expression. However, invasive cells also require a more malleable nucleus, and exploring the pathways that bring about this structural change to the nuclear periphery represent potential targets for intervention to destroy the cell.

The MCF7 cell line is derived from a poorly invasive carcinoma (Z. Liu, Brattain, & Appert, 1997) and provides a background of malignant pathway activation against which phenotypic nuclear changes resulting from HP1α loss were observed. Reduction of HP1α expression reduced the mechanical integrity of the MCF7 cell nucleus, decreasing resistance to shear forces by over 60% (Figure 16**)** and greatly increased nuclear elasticity, decreasing the stiffness of the control cell nuclei Youngs modulus of 19kPa to 2.5kPa, at 0.5nN applied pressure by atomic force microscopy (Figure 19). The Youngs modulus was calculated over a range of applied forces, in order to gather representative date over a force scale such that it may be compared with data collected with alternate techniques. Additionally, loss of HP1α reduced the internal complexity of the nuclei, observed as a loss of heterogeneity of cell elasticity across multiple points across the surface of the sampled cells (Figure B). This variation in resistance to pressure can be inferred as changes to the underlying nuclear lamina and peripheral heterochromatin that provide support to the nuclear membrane. Using the atomic force microscopy data as a baseline, there are ongoing collaborations from this project to calibrate additional techniques, micro-aspiration or optical tweezer manipulation, for measuring nuclear elasticity. Micro-aspiration involves using fixed pressure through a micro-pipette held directly against a membrane, and the physical degree to which the membrane is drawn into the pipette can be used to compare and quantify the elastic properties of the membrane between cell types or isolated nuclei (Dahl et al., 2005).

The main determinant of nuclear envelope rigidity is the underlying nuclear lamina meshwork which abuts peripheral heterochromatin. Asynchronous MCF7 cells demonstrated clear

morphological changes to the lamin A/C network following HP1α reduction, with this network beneath the nuclear membrane markedly crumpled and distorted, indicating detachment and disorganization of this lamina layer (Figure 20). Lamin B2 did not exhibit the same degree of disruption to the meshwork as lamins A/C although an increase in punctate foci within the nucleus was observed in HP1α KD cells. Lamin B2 may be less prone to detachment from the inner nuclear membrane than the type A lamin family, as B-type lamins undergo permanent farnesylation, a binding moiety that targets and binds them to the interior of the membrane. A-type lamins are only transiently farnesylated (Vorburger, Kitten, & Nigg, 1989).

As the total protein and total nuclear protein for lamin A/C, and B2 are equivalent between MCF7 cells with HP1α, this demonstrates both lamin families are still targeted to the nuclear membrane in cells with reduced HP1α, but the lamina is less stable. To further explore this relationship, the lamins A, C, and B2 were tested for their comparative solubility from isolated whole nuclei following HP1α KD. In particular, lamin A and C were more soluble at low salt concentrations, with lamin A increased solubility in 250mM NaCl compared to the MCF7 nuclei. Lamin A is known to interact directly with DNA, so disruption of the peripheral heterochromatin structures maintained by HP1α polymerization is a possible mechanism by which this disruption occurs. Imaging of the nuclear periphery to identify co-localization of lamin A/C with peripheral heterochromatin, was explored using immuno-labelled transmission electron microscopy, however optimization of this technique is ongoing. Transmission electron microscopy of agar-embedded asynchronous MCF7 control and HP1α KD cells demonstrated broad rearrangement of the peripheral heterochromatin, with large well-defined regions of dense chromatin visible around the nuclear periphery of control cells. By contrast, the chromatin of the HP1α KD cells is far more heterogenous, with few distinguishable regions of grouped heterochromatin. This data reflects the results of the atomic force microscopy maps of cell, illustrating the major rearrangement of nuclear material, both chromatin and lamina, and reducing mechanical rigidity of the nucleus.

An increase in the solubility lamin B2, although not to the same extent as that of lamin A/C (Figure 25B) is also observed in cells with reduced HP1α expression. The lamin B family is more firmly associated with the nuclear membrane, having a secondary N-terminal binding domain that interacts with LBR, and results in lamin B proteins being anchored at either end leading to a more stable interaction. In MCF7 nuclei, LBR was observed to be localized to the

inner nuclear membrane, in addition to a faint presence in the cytoplasm, as previously observed in MCF7 cells (Figure 28B) (Zwerger, Kolb, Richter, Karakesisoglou, & Herrmann, 2010). However, in cells with reduced HP1α there is no observable cytoplasmic LBR, and an increase in nuclear localization, although total protein expression is unchanged (Figure 23C). As LBR is recruited to the nuclear membrane during nuclear envelope formation, mediated by importin β, disruption to the correct formation of the membrane and underlying lamina caused by chromatin lacking HP1α could promote increased nuclear import of LBR (Pajerowski, Dahl, Zhong, Sammak, & Discher, 2007).

In general, HP1α reduction has a marked effect on the ability of the nuclear membrane to retain associated proteins, including the lamins, LBR and nesprin. There is evidence from co-immunoprecipitation and immunofluorescence trials that lamin C and emerin are dependent on lamin A for organization at the membrane, and so loss of correct lamin A function, as observed in the MCF7 HP1α KD cells would result in a cascading disruption the nuclear lamina and its associated proteins (Vaughan et al., 2001). (Vaughan et al., 2001) also describe that loss of functional lamin A resulted in the formation of formation emerin aggregates within the endoplasmic reticulum, which was observed here following HP1α KD (Figure 30A).
Mass spectroscopy was used to identify proteins that showed clear changes in protein concentration in the enriched nuclear membrane lysate from MCF7 cells without HP1α. In addition to loss of lamin B1 following HP1α KD, there was increased detection of VDAC1 protein in the membrane (Figure 29). VDAC1 is a voltage dependent nuclear membrane channel required for the nuclear import of acidic fibroblast growth factor, which is a mitogenic cell growth factor that can encourage endothelial cell migration and proliferation (Yamanaka et al., 1993). Further investigation of whether functional aFGF is present in the nucleus following HP1α will be carried out in future work.

In summary, reduction of HP1α results in a significant reduction in nuclear membrane stiffness and integrity, a key determining factor in the onset of malignant behaviour, as demonstrated in the *Drosophila* model. It is shown here that loss of HP1α results in wide disorganisation of the nuclear lamina and peripheral heterochromatin, which directly influence membrane stability. In particular, targeting and retention of lamin A to the nuclear membrane is greatly reduced, which presumably has cascading disruptive effects on other nuclear membrane associated proteins.

References

Abràmoff, M. D., Magalhães, P. J., & Ram, S. J. (2004). Image processing with ImageJ. *Biophotonics international, 11*(7), 36-42.

Bussolati, G., Marchiò, C., Gaetano, L., Lupo, R., & Sapino, A. (2008). Pleomorphism of the nuclear envelope in breast cancer: a new approach to an old problem. *Journal of cellular and molecular medicine, 12*(1), 209-218.

Contreras, A., Gutierrez, M. C., & Hale, T. K. (2010). Differential Expression Patterns of the Heterochromatin Proteins HP1 alpha and HP1 beta in Different Tumor Types. *Modern Pathology, 23*, 385A-385A.

Dahl, K. N., Engler, A. J., Pajerowski, J. D., & Discher, D. E. (2005). Power-law rheology of isolated nuclei with deformation mapping of nuclear substructures. *Biophysical journal, 89*(4), 2855-2864.

Dahl, K. N., Kahn, S. M., Wilson, K. L., & Discher, D. E. (2004). The nuclear envelope lamina network has elasticity and a compressibility limit suggestive of a molecular shock absorber. *Journal of Cell Science, 117*(20), 4779-4786.

De Koning, L., Savignoni, A., Boumendil, C., Rehman, H., Asselain, B., Sastre-Garau, X., & Almouzni, G. (2009). Heterochromatin protein 1alpha: a hallmark of cell proliferation relevant to clinical oncology. *EMBO Mol Med, 1*(3), 178-191. doi:10.1002/emmm.200900022

Dechat, T., Adam, S. A., Taimen, P., Shimi, T., & Goldman, R. D. (2010). Nuclear Lamins. *Cold Spring Harbor perspectives in biology, 2*(11), a000547. doi:10.1101/cshperspect.a000547

Denais, C. M., Gilbert, R. M., Isermann, P., McGregor, A. L., te Lindert, M., Weigelin, B., . . . Lammerding, J. (2016). Nuclear envelope rupture and repair during cancer cell migration. *Science*, aad7297.

Deng, Z., Campbell, A. E., & Lieberman, P. M. (2010). TERRA, CpG methylation, and telomere heterochromatin: lessons from ICF syndrome cells. *Cell Cycle, 9*(1), 69-74.

Deng, Z., Norseen, J., Wiedmer, A., Riethman, H., & Lieberman, P. M. (2009). TERRA RNA binding to TRF2 facilitates heterochromatin formation and ORC recruitment at telomeres. *Molecular cell, 35*(4), 403-413.

Eissenberg, J. C., James, T. C., Foster-Hartnett, D. M., Hartnett, T., Ngan, V., & Elgin, S. (1990). Mutation in a heterochromatin-specific chromosomal protein is associated with suppression of position-effect variegation in Drosophila melanogaster. *Proceedings of the National Academy of Sciences, 87*(24), 9923-9927.

Furusawa, T., Rochman, M., Taher, L., Dimitriadis, E. K., Nagashima, K., Anderson, S., & Bustin, M. (2015). Chromatin decompaction by the nucleosomal binding protein HMGN5 impairs nuclear sturdiness. *Nature communications, 6*, 6138.

Groth, A. C., Fish, M., Nusse, R., & Calos, M. P. (2004). Construction of transgenic Drosophila by using the site-specific integrase from phage φC31. *Genetics, 166*(4), 1775-1782.

Haaf, T., & Schmid, M. (2000). Experimental condensation inhibition in constitutive and facultative heterochromatin of mammalian chromosomes. *Cytogenetic and Genome Research, 91*(1-4), 113-123.

Hale, T. K., Wheeler, D., Stimpson, L., Tretiakova, M. S., & Contreras, A. (2016). Loss of HP1alpha promotes cell invasion in breast tumours. *Cancer research, Sumitted.*

Harada, T., Swift, J., Irianto, J., Shin, J.-W., Spinler, K. R., Athirasala, A., . . . Discher, D. E. (2014). Nuclear lamin stiffness is a barrier to 3D migration, but softness can limit survival. *J Cell Biol*, jcb. 201308029.

Hutchison, C. J., Alvarez-Reyes, M., & Vaughan, O. A. (2001). Lamins in disease: why do ubiquitously expressed nuclear envelope proteins give rise to tissue-specific disease phenotypes? *Journal of Cell Science, 114*(1), 9-19.

James, T. C., & Elgin, S. (1986). Identification of a nonhistone chromosomal protein associated with heterochromatin in Drosophila melanogaster and its gene. *Molecular and cellular biology, 6*(11), 3862-3872.

Janmey, P. A., Euteneuer, U., Traub, P., & Schliwa, M. (1991). Viscoelastic properties of vimentin compared with other filamentous biopolymer networks. *The Journal of cell biology, 113*(1), 155-160.

Kirschmann, D. A., Lininger, R. A., Gardner, L. M., Seftor, E. A., Odero, V. A., Ainsztein, A. M., . . . Hendrix, M. J. (2000). Down-regulation of HP1Hsalpha expression is associated with the metastatic phenotype in breast cancer. *Cancer Res, 60*(13), 3359-3363.

Kirschmann, D. A., Lininger, R. A., Gardner, L. M., Seftor, E. A., Odero, V. A., Ainsztein, A. M., . . . Hendrix, M. J. (2000). Down-regulation of HP1Hsα expression is associated with the metastatic phenotype in breast cancer. *Cancer research, 60*(13), 3359-3363.

Kirschmann, D. A., Seftor, E. A., Nieva, D. R., Mariano, E. A., & Hendrix, M. J. (1999). Differentially expressed genes associated with the metastatic phenotype in breast cancer. *Breast cancer research and treatment, 55*(2), 125-134.

Kitamura, T., Qian, B.-Z., & Pollard, J. W. (2015). Immune cell promotion of metastasis. *Nature Reviews Immunology, 15*(2), 73-86.

Kuga, T., Nozaki, N., Matsushita, K., Nomura, F., & Tomonaga, T. (2010). Phosphorylation statuses at different residues of lamin B2, B1, and A/C dynamically and independently change throughout the cell cycle. *Experimental cell research, 316*(14), 2301-2312.

Lai, X., Deng, Z., Guo, H., Zhu, X., & Tu, W. (2017). HP1alpha is highly expressed in glioma cells and facilitates cell proliferation and survival. *Biochem Biophys Res Commun, 490*(2), 415-422. doi:10.1016/j.bbrc.2017.06.056

Larson, A. G., Elnatan, D., Keenen, M. M., Trnka, M. J., Johnston, J. B., Burlingame, A. L., . . . Narlikar, G. J. (2017). Liquid droplet formation by HP1α suggests a role for phase separation in heterochromatin. *Nature, 547*(7662), 236.

Li, L., & Li, W. (2015). Epithelial–mesenchymal transition in human cancer: comprehensive reprogramming of metabolism, epigenetics, and differentiation. *Pharmacology & therapeutics, 150*, 33-46.

Liu, M., Huang, F., Zhang, D., Ju, J., Wu, X. B., Wang, Y., . . . Zhao, Q. (2015). Heterochromatin protein HP1gamma promotes colorectal cancer progression and is regulated by miR-30a. *Cancer Res, 75*(21), 4593-4604. doi:10.1158/0008-5472.CAN-14-3735

Liu, Z., Brattain, M. G., & Appert, H. (1997). Differential display of reticulocalbin in the highly invasive cell line, MDA-MB-435, versus the poorly invasive cell line, MCF-7. *Biochemical and biophysical research communications, 231*(2), 283-289.

Meehan, R. R., Kao, C. F., & Pennings, S. (2003). HP1 binding to native chromatin in vitro is determined by the hinge region and not by the chromodomain. *The EMBO journal, 22*(12), 3164-3174.

Nishibuchi, G., & Nakayama, J.-i. (2014). Biochemical and structural properties of heterochromatin protein 1: understanding its role in chromatin assembly. *The Journal of Biochemistry, 156*(1), 11-20.

Nishimura, K., Hirokawa, Y. S., Mizutani, H., & Shiraishi, T. (2006). Reduced

Heterochromatin Protein 1-beta (HP1β) Expression is Correlated with Increased Invasive Activity in Human Melanoma Cells. *Anticancer research, 26*(6B), 4349-4356.

Norwood, L. E., Grade, S. K., Cryderman, D. E., Hines, K. A., Furiasse, N., Toro, R., . . . Hendrix, M. J. (2004). Conserved properties of HP1 Hsα. *Gene, 336*(1), 37-46.

Norwood, L. E., Moss, T. J., Margaryan, N. V., Cook, S. L., Wright, L., Seftor, E. A., . . . Wallrath, L. L. (2006). A requirement for dimerization of HP1Hsα in suppression of breast cancer invasion. *Journal of Biological Chemistry, 281*(27), 18668-18676.

Olins, A. L., Zwerger, M., Herrmann, H., Zentgraf, H., Simon, A. J., Monestier, M., & Olins, D. E. (2008). The human granulocyte nucleus: Unusual nuclear envelope and heterochromatin composition. *European journal of cell biology, 87*(5), 279-290.

Ornitz, D. M., Moreadith, R. W., & Leder, P. (1991). Binary system for regulating transgene expression in mice: targeting int-2 gene expression with yeast GAL4/UAS control elements. *Proceedings of the National Academy of Sciences, 88*(3), 698-702.

Pajerowski, J. D., Dahl, K. N., Zhong, F. L., Sammak, P. J., & Discher, D. E. (2007). Physical plasticity of the nucleus in stem cell differentiation. *Proceedings of the National Academy of Sciences of the United States of America, 104*(40), 15619-15624. doi:10.1073/pnas.0702576104

Peters, A. H., O'Carroll, D., Scherthan, H., Mechtler, K., Sauer, S., Schöfer, C., . . . Kohlmaier, A. (2001). Loss of the Suv39h histone methyltransferases impairs mammalian heterochromatin and genome stability. *Cell, 107*(3), 323-337.

Pomeroy, S. L., Tamayo, P., Gaasenbeek, M., Sturla, L. M., Angelo, M., McLaughlin, M. E., . . . Golub, T. R. (2002). Prediction of central nervous system embryonal tumour outcome based on gene expression. *Nature, 415*(6870), 436-442.

Rea, S., Eisenhaber, F., O'Carroll, D., Strahl, B. D., Sun, Z.-W., Schmid, M., . . . Allis, C. D. (2000). Regulation of chromatin structure by site-specific histone H3 methyltransferases. *Nature, 406*(6796), 593-599.

Ritou, E., Bai, M., & Georgatos, S. D. (2007). Variant-specific patterns and humoral regulation of HP1 proteins in human cells and tissues. *J Cell Sci, 120*(Pt 19), 3425-3435. doi:jcs.012955 [pii]
10.1242/jcs.012955

Ruginis, T., Taglia, L., Matusiak, D., Lee, B. S., & Benya, R. V. (2006). Consequence of gastrin-releasing peptide receptor activation in a human colon cancer cell line: A proteomic approach. *Journal of Proteome Research, 5*(6), 1460-1468. doi:10.1021/pr060005g

Shapiro, E., Huang, H., Ruoff, R., Lee, P., Tanese, N., & Logan, S. K. (2008). The heterochromatin protein 1 family is regulated in prostate development and cancer. *J Urol, 179*(6), 2435-2439. doi:S0022-5347(08)00238-3 [pii]
10.1016/j.juro.2008.01.091

Shi, S., Calhoun, H. C., Xia, F., Li, J., Le, L., & Li, W. X. (2006). JAK signaling globally counteracts heterochromatic gene silencing. *Nature genetics, 38*(9), 1071-1076.

Shimi, T., Pfleghaar, K., Kojima, S.-i., Pack, C.-G., Solovei, I., Goldman, A. E., . . . Cremer, T. (2008). The A-and B-type nuclear lamin networks: microdomains involved in chromatin organization and transcription. *Genes & development, 22*(24), 3409-3421.

Shiota, M., Song, Y., Yokomizo, A., Tada, Y., Kuroiwa, K., Eto, M., . . . Naito, S. (2010). Human heterochromatin protein 1 isoform HP1beta enhances androgen receptor activity and is implicated in prostate cancer growth. *Endocr Relat Cancer, 17*(2), 455-467. doi:10.1677/ERC-09-0321

Solomon, R. (2016). *Heterochromatin Protein 1α can regulate epithelial cell invasion in vivo.* (Honours), Manawatu, Palmerston North.

Spratford, C. M., & Kumar, J. P. (2014). Dissection and immunostaining of imaginal discs from Drosophila melanogaster. *Journal of visualized experiments: JoVE*(91), 51792.

Sullivan, T., Escalante-Alcalde, D., Bhatt, H., Anver, M., Bhat, N., Nagashima, K., . . . Burke, B. (1999). Loss of A-type lamin expression compromises nuclear envelope integrity leading to muscular dystrophy. *The Journal of cell biology, 147*(5), 913-920.

Tell, R., Rivera, C. A., Eskra, J., Taglia, L. N., Blunier, A., Wang, Q. T., & Benya, R. V. (2011). Gastrin-releasing peptide signaling alters colon cancer invasiveness via heterochromatin protein 1Hsbeta. *The American journal of pathology, 178*(2), 672-678. doi:10.1016/j.ajpath.2010.10.017

Tretiakova, M. S., Bond, S. D., Wheeler, D., Contreras, A., Kocherginsky, M., Kroll, T. G., & Hale, T. K. (2014). Heterochromatin protein 1 expression is reduced in human thyroid malignancy. *Lab Invest, 94*(7), 788-795. doi:10.1038/labinvest.2014.68

Vaughan, O. A., Alvarez-Reyes, M., Bridger, J. M., Broers, J. L. V., Ramaekers, F. C. S., Wehnert, M., . . . Hutchison, C. J. (2001). Both emerin and lamin C depend on lamin A for localization at the nuclear envelope. *Journal of Cell Science, 114*(14), 2577.

Vidal, M., Larson, D. E., & Cagan, R. L. (2006). Csk-deficient boundary cells are eliminated from normal *Drosophila* epithelia by exclusion, migration, and apoptosis. *Developmental cell, 10*(1), 33-44.

Vlcek, S., Dechat, T., & Foisner, R. (2001). Nuclear envelope and nuclear matrix: interactions and dynamics. *Cellular and Molecular Life Sciences CMLS, 58*(12-13), 1758-1765.

Vorburger, K., Kitten, G., & Nigg, E. (1989). Modification of nuclear lamin proteins by a mevalonic acid derivative occurs in reticulocyte lysates and requires the cysteine residue of the C-terminal CXXM motif. *The EMBO journal, 8*(13), 4007-4013.

Wasenius, V. M., Hemmer, S., Kettunen, E., Knuutila, S., Franssila, K., & Joensuu, H. (2003). Hepatocyte growth factor receptor, matrix metalloproteinase-11, tissue inhibitor of metalloproteinase-1, and fibronectin are up-regulated in papillary thyroid carcinoma: a cDNA and tissue microarray study. *Clin Cancer Res, 9*(1), 68-75.

Yamanaka, Y., Friess, H., Buchler, M., Beger, H. G., Uchida, E., Onda, M., . . . Korc, M. (1993). Overexpression of Acidic and Basic Fibroblast Growth Factors in Human Pancreatic Cancer Correlates with Advanced Tumor Stage. *Cancer research, 53*(21), 5289.

Zhang, Q., Skepper, J. N., Yang, F., Davies, J. D., Hegyi, L., Roberts, R. G., . . . Shanahan, C. M. (2001). Nesprins: a novel family of spectrin-repeat-containing proteins that localize to the nuclear membrane in multiple tissues. *Journal of Cell Science, 114*(24), 4485-4498.

Zwerger, M., Kolb, T., Richter, K., Karakesisoglou, I., & Herrmann, H. (2010). Induction of a Massive Endoplasmic Reticulum and Perinuclear Space Expansion by Expression of Lamin B Receptor Mutants and the Related Sterol Reductases TM7SF2 and DHCR7. *Molecular biology of the cell, 21*(2), 354-368. doi:10.1091/mbc.e09-08-0739